American Mineralogist, Volume 58, pages 594–618, 1973

High-Temperature Crystal Chemistry of Acmite, Diopside, Hedenbergite, Jadeite, Spodumene, and Ureyite

MARYELLEN CAMERON, SHIGEHO SUENO, C. T. PREWITT, AND J. J. PAPIKE

Department of Earth and Space Sciences, State University of New York, Stony Brook, New York 11790

Abstract

Crystal structure parameters have been determined for acmite, $NaFe^{3+}Si_2O_6$ (at ~400°C, 600°C, 800°C), diopside, $CaMgSi_2O_6$ (at ~400°C, 700°C, 850°C, 1000°C), hedenbergite, $CaFe^{2+}Si_2O_6$ (at ~24°C, 400°C, 600°C, 800°C, 900°C, 1000°C), jadeite, $NaAlSi_2O_6$ (at ~24°C, 400°C, 600°C, 800°C), spodumene, $LiAlSi_2O_6$ (at ~300°C, 460°C, 760°C) and ureyite, $NaCrSi_2O_6$ (at ~400°C, 600°C). Refinements in space group $C2/c$ using anisotropic temperature factors and over 640 reflections for each set of data resulted in unweighted R-factors ranging from 0.022 to 0.078.

The increase in mean Si–O bond lengths with increasing temperature is not statistically significant, but the mean M–O distances for both the 6- and 8-coordinated sites in the six pyroxenes exhibit relatively large increases. The mean thermal expansion coefficients for the various bonds increase in the following order: Si^{4+}–O < Cr^{3+}–O < Fe^{3+}–O < Al^{3+}–O < Fe^{2+}–O < Na^{+}–O < Mg^{2+}–O < Ca^{2+}–O < Li^{+}–O. This series is essentially a function of decreasing bond strength, although the position of Mg^{2+}–O may indicate an exception to this trend. The pyroxene structures accommodate the differential mean M–O expansions through (1) extension of the silicate tetrahedral chains, (2) distortion of the silicate tetrahedra, and (3) an increase in out-of-plane tilting of silicate tetrahedra. In all six minerals thermal expansion is accomplished principally by expansion of the non-tetrahedral polyhedra with concomitant expansion of the voids between the cation polyhedra, and rotation of the fairly rigid tetrahedra about the bridging oxygen atoms. The rate of increase of the equivalent isotropic temperature factor for a cation is generally proportional to the coordination number of that cation.

Introduction

Although the basic structure of clinopyroxenes was determined almost 45 years ago (Warren and Bragg, 1928), the structural details are still being investigated. Within the last 10 years many excellent refinements of structures using intensity data collected at room temperature have become available (*e.g.*, for end-member compositions: Christensen and Hazell, 1967; Freed and Peacor, 1967; Clark, Appleman, and Papike, 1969), and the results have been extensively used by workers interested in phenomena such as phase transitions, exsolution, solid solution and intracrystalline equilibria that take place above room temperature. Since the extrapolation of room-temperature structural data to higher temperatures is uncertain, it is important to examine the structures of pyroxenes while the crystals are held at high temperatures. This type of structural data provides information on the high-temperature phenomena mentioned above and, in addition, should provide valuable insight into the mechanisms of anisotropic thermal expansion. Published refinements of pyroxene structures using intensity data collected at high temperatures include those of Smyth (1971; protoenstatite), Smyth and Burnham (1972; clinohypersthene), and Brown, Prewitt, Papike, and Sueno (1972; pigeonite).

In this study we have examined the structures of six $C2/c$ pyroxenes (spodumene,[1] $LiAlSi_2O_6$; jadeite, $NaAlSi_2O_6$; acmite, $NaFe^{3+}Si_2O_6$; ureyite, $NaCrSi_2O_6$; diopside, $CaMgSi_2O_6$; and hedenbergite $CaFe^{2+}Si_2O_6$) at a series of temperatures ranging from room temperature up to 1000°C (Table A-1).[2] End-member

[1] May actually be $C2$.

[2] Table numbers preceded by the letter "A" are located in the Appendix at the end of the paper. The absence of a prefix indicates that the table can be located in the text of the paper.

pyroxenes were selected in order to study thermal expansion of each cation uniquely and to avoid effects of mixed site populations. The upper temperature limits for the series of intensity collections for individual minerals were determined by pyroxene stabilities and furnace capabilities. The new room-temperature refinements presented herein for jadeite and hedenbergite are in close agreement with those previously published by Prewitt and Burnham (1966; jadeite) and Veblen and Burnham (1969; hedenbergite). Room-temperature refinements of spodumene, acmite, ureyite, and diopside of Clark *et al* (1969) were used for comparison with our high-temperature data. We will specifically consider the variation with increasing temperature of cell parameters, interatomic distances, polyhedral volumes, and thermal parameters and then, on the basis of these results, attempt to explain some mechanisms of thermal expansion in pyroxenes.

Experimental Data

Chemical and Crystallographic Data

Except for hedenbergite, all of the crystals used in the structural studies presented herein were obtained from samples previously used by Prewitt and Burnham (1966; jadeite) and Clark *et al* (1969; spodumene, acmite, diopside, and ureyite) in their room-temperature refinements. Jadeite, spodumene, acmite, and diopside are natural specimens but they closely approximate end-member pyroxene compositions (for chemical data see Prewitt and Burnham, 1966, and Clark *et al,* 1969). The ureyite was synthesized by L. Fuchs from a melt of $NaCr^{3+}Si_2O_6$ plus 10 wt percent Na_2SiO_3 in air at 1000°C for 2 days. The hedenbergite was synthesized by D. H. Lindsley at approximately 980°C and 20 kbars for 8 hours.

The pyroxene specimens were oriented parallel to c^* on Suprasil quartz glass fibers with a high-temperature cement composed of solid Al_2O_3 combined with a liquid binder. To prevent oxidation of the Fe^{2+} in hedenbergite, the crystal was placed in an evacuated silica capillary following the procedure described by Brown, Sueno, and Prewitt (1973). Except in the initial stages of our high-temperature study (*i.e.,* during the diopside data collection), one crystal was used to collect the complete series of intensities at various temperatures for each pyroxene. In most instances data collection began within 8 hours after the desired temperatures had been obtained. The temperature uncertainty depends on the crystal temperature and is approximately ±20°C (Brown *et al,* 1973).

X-Ray Diffraction Data

Using data collected on the Picker diffractometer, unit cell parameters were determined by measurement of 2θ values of 15 to 20 reflections, principally of the type *hkl*. Refinement of these 2θ values in the PODEX2 program written by A. W. Sleight[3] yielded the cell parameters listed in Table A-2. No corrections for systematic errors were included in the refinements.

Between 800 and 950 independent intensities were collected at each temperature (Table A-1) using a PDP 15/35-controlled Picker diffractometer. Diffractometer settings were calculated using the GSET program coded by C. T. Prewitt. To maintain uniformity, we attempted to collect the same set of reflections within $2\theta = 10°$–$65°$ for each structure. The Picker diffractometer was operated in an $\omega - 2\theta$ mode using a graphite monochromater and Mo$K\alpha$ radiation. The scan range was varied from 2° to 2.5°, being increased at higher temperature because of peak broadening. Five-second background counts were taken on both sides of each peak. A standard reflection 060 was monitored throughout each data collection. It was repeated every 20 reflections and its structure factor usually varied by less than one standard deviation. No absorption corrections were made for any of the pyroxenes due to their small size (<0.1 mm in cross section) and small linear absorption coefficients for Mo radiation.[4]

Both isotropic and anisotropic refinements were calculated for each set of intensity data in space group $C2/c$[5] using neutral atom scattering factors[4] (Doyle and Turner, 1968), unit weights[4] and the RFINE program written by L. W. Finger. Starting parameters for hedenbergite were those of diopside, whereas previously published room-temperature parameters were used for the remaining five pyroxenes.

[3] Central Research Department, E. I. duPont de Nemours and Company, Wilmington, Delaware.

[4] Our experience has shown that the use of absorption corrections and different weighting schemes and scattering factor curves for these minerals has very little effect on final results of the refinements, providing that significant systematic errors resulting from improper experimental techniques are not present in the data.

[5] No reflections violating $C2/c$ space group symmetry were observed in precession photographs of any of the crystals, including spodumene.

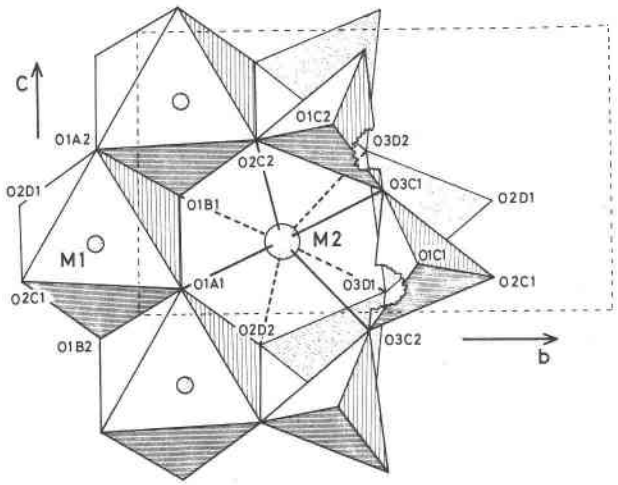

FIG. 1. The $C2/c$ pyroxene structure projected down a^*. Nomenclature is consistent with that of Burnham *et al* (1967).

Observed structure factors and the β_{ij}'s from the final cycle of each anisotropic refinement may be ordered as NAPS document #02120.[6] Final positional and thermal parameters determined from the anisotropic refinements are given in the Appendix (Table A-3). R-factors for these anisotropic refinements of the 22 new sets of data range from 0.025 to 0.078 (Table A-1). The high values of the R-factors for ureyite are not the result of experimental difficulties during collection of the intensity data, but are due to the relatively poor quality of the crystal used. Selected interatomic distances, angles, thermal ellipsoids and their associated errors, calculated using the ERROR program of L. W. Finger, are listed in the Appendix (Table A-4: Si–O interatomic distances; Table A-5: tetrahedral O–O distances; Table A-6: tetrahedral angles; Table A-7: $M(1)$–O interatomic distances; Table A-8: octahedral O–O distances; Table A-9: octahedral angles; Table A-10: $M(2)$–O interatomic distances; Table A-11: magnitudes and orientations of thermal ellipsoids). Although thermal corrections for interatomic distances may be advisable, we have not made such corrections because of uncertainty in selecting a model which adequately describes the thermal motion effect on bond distances in the pyroxene structure. Except for plots involving β, the slopes of all lines in the figures were determined with a linear least-squares computer program.

[6] Microfiche Publications, 305 East 46th Street, New York, N.Y. 10017. Please remit in advance $1.50 for microfiche or $40.10 for photocopies (264 pages). Please check the most recent issue of this journal for the current address and prices.

Thermal Expansion Terminology

The mean thermal expansion coefficient

$$\alpha_X = \frac{1}{X_{24}} \cdot \frac{X_T - X_{24}}{T - 24},$$

is used throughout this study to characterize thermal expansions of selected parameters. The terms X_{24} and X_T are the values of the parameter at 24°C [room temperature] and at some higher temperature T. The quantity α_X represents a percentage increase per degree (actually percent $\times$ 10^{-2}/degree) over the temperature range studied, and algebraically it is equivalent to the rate of increase with temperature divided by the room temperature value of the parameter. In actual practice each α was calculated by dividing the slope obtained from least-squares analysis,

$$\frac{X_T - X_{24}}{T - 24},$$

by the value of the parameter at room temperature. We have occasionally used rate of increase rather than α_X, the mean thermal expansion coefficient, when describing some of the data displays since the

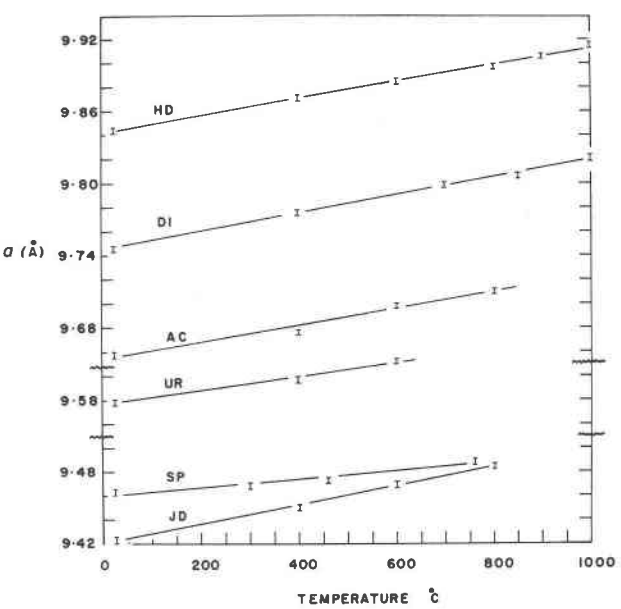

FIG. 2. Variation of a unit cell parameter with increasing temperature for six clinopyroxenes. Abbreviations: HD = hedenbergite, DI = diopside, AC = acmite, UR = ureyite, JD = jadeite, SP = spodumene. Error bars represent ±1 standard deviation.

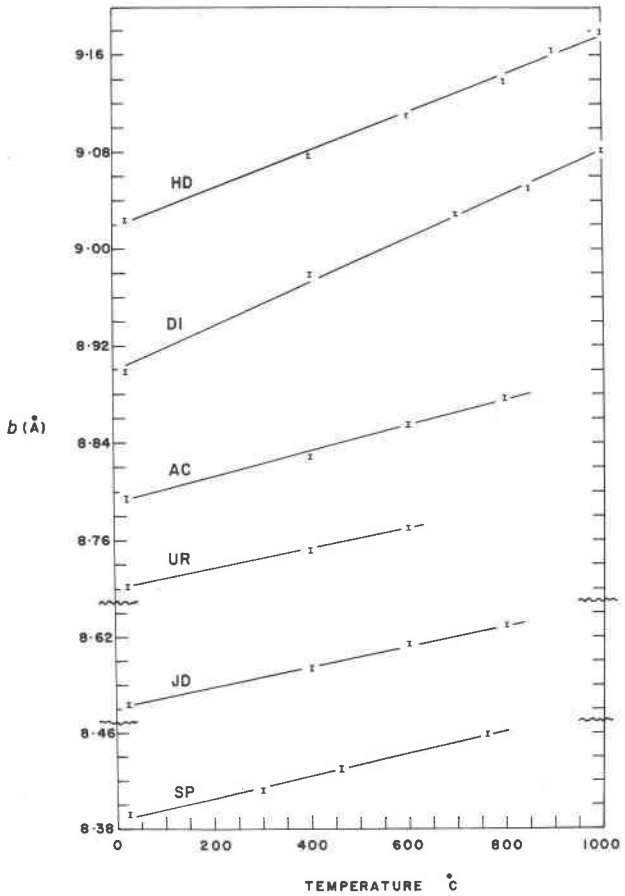

FIG. 3. Variation of b unit cell parameter with increasing temperature for six clinopyroxenes. (Abbreviations are the same as those in Figure 2.) Error bars represent ±1 standard deviation.

rate of increase (*i.e.*, the slope) is directly observable on these plots.

The Pyroxene Structure

Figure 1 shows a projection of the $C2/c$ pyroxene structure along a^*. The $M(1)$ site, which is octahedrally coordinated, is occupied by Al (spodumene and jadeite), Fe^{3+} (acmite), Cr^{3+} (ureyite), Mg (diopside) or Fe^{2+} (hedenbergite). The larger $M(2)$ site is either 6- or 8-coordinated and is occupied by Ca (diopside and hedenbergite), Na (jadeite, acmite, and ureyite) or Li (spodumene). There is only one type of tetrahedral site, and it is completely occupied by silicon in all six pyroxenes examined. There are three crystallographically non-equivalent oxygen atoms, O(1), O(2) and O(3). O(3) is referred to as a bridging oxygen in that it is bonded to two silicon atoms, whereas O(1) and O(2) are both

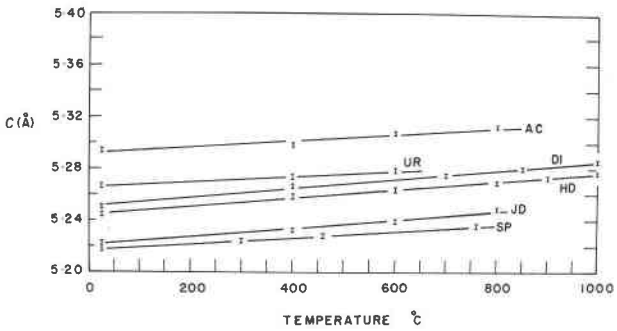

FIG. 4. Variation of c unit cell parameter with increasing temperature for six clinopyroxenes. (Abbreviations are the same as those in Figure 2.) Error bars represent ±1 standard deviation.

non-bridging oxygens. The O(3)–O(3)–O(3) angle is used as a measure of the extension of the silicate chain. For further details of the clinopyroxene structure, the reader is referred to the paper by Clark *et al* (1969). The nomenclature used throughout this paper is consistent with that proposed by Burnham, Clark, Papike, and Prewitt (1967).

Unit Cell Parameters

The variations in unit cell parameters as a function of temperature (Figs. 2–6) are linear with the exception of the β angles in diopside and hedenbergite. Examination of the mean thermal expansion coefficients of the cell parameters (Table 1) reveals that $\alpha_b > \alpha_a > \alpha_c$ for all pyroxenes except spodumene. Expansions along d_{100} ($\equiv a^*$) (Fig. 7) are of interest because this is the direction perpen-

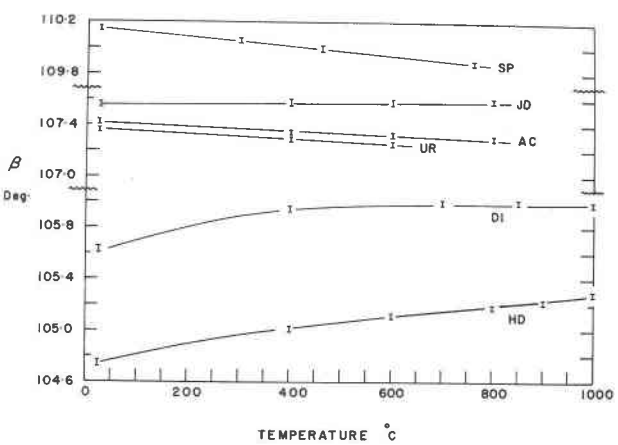

FIG. 5. Variation of β with increasing temperature for six clinopyroxenes. (Abbreviations are the same as those in Figure 2.) Error bars represent ±1 standard devation.

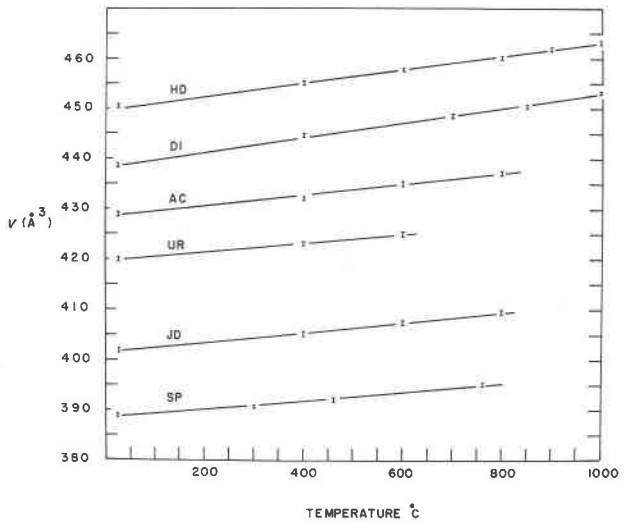

FIG. 6. Variation of unit cell volume with increasing temperature for six clinopyroxenes. (Abbreviations are the same as those in Figure 2.) Error bars represent ±1 standard deviation.

dicular to the octahedral layers and, as such, should be a better parameter with which to compare the expansions along *b*. The mean thermal expansion coefficients in this direction are also less than those in the *b* directions and they are quite similar to *c* in both diopside and hedenbergite. Both the rate of increase and the mean thermal expansion for the *b* cell parameters are significantly greater for the two

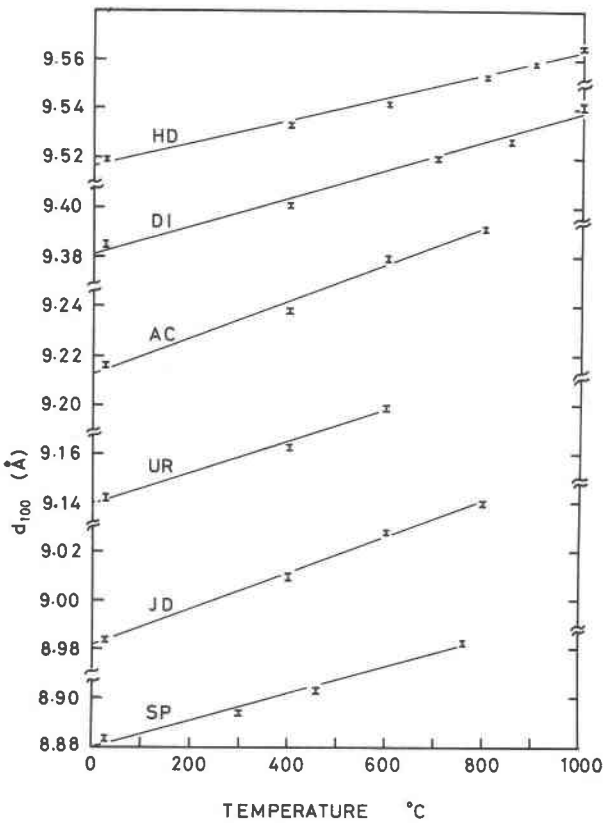

FIG. 7. Variation of d_{100} with increasing temperature for six clinopyroxenes. (Abbreviations are the same as those in Figure 2.) Error bars represent ±1 standard deviation.

TABLE 1. Mean Thermal Expansion Coefficients ($°C^{-1} \times 10^5$) of Unit Cell Parameters*

	Spodumene (24-760°C)	Jadeite (24-800°C)	Acmite (24-800°C)	Ureyite (24-600°C)	Diopside (24-1000°C)	Hedenbergite (24-1000°C)
α_a	0.380**	0.850	0.727	0.585	0.779	0.724
$\alpha_{d_{100}}$	0.600	0.817	0.804	0.691	0.606	0.483
α_b	1.11	1.00	1.20	0.946	2.05	1.76
α_c	0.475	0.631	0.450	0.390	0.646	0.597
α_v	2.22	2.47	2.47	2.04	3.33	2.98
α_{v-p}***	2.03	2.07	2.30	1.61	2.91	2.46
α_p****	2.83	3.09	2.78	2.79	3.97	3.45

*Mean thermal expansion coefficients α are computed from the equation $\alpha_X = \frac{1}{X_{24}} \cdot \frac{X_T - X_{24}}{T-24}$, where the slope of the regression equation is used for the term $\frac{X_T - X_{24}}{T-24}$. See text of paper.

**For 0.380, read $0.380 \times 10^{-5}\ C^{-1}$.

***v-p is the volume of space between the cation polyhedra.

****p is the polyhedral volume determined by summing the volumes of all polyhedra within a unit cell.

calcic pyroxenes (Figure 3 and Table 1). With increasing temperature, the β angle in the sodic pyroxenes and spodumene either decreases or remains approximately constant whereas in the calcic pyroxenes it increases non-linearly. Mean thermal expansion coefficients (Table 1) and plots of the change in unit cell volumes (Fig. 6) as a function of temperature both indicate that diopside and hedenbergite exhibit higher rates of thermal expansion than either spodumene or the sodic pyroxenes.

Polyhedral Expansions

Silicate Tetrahedra

Mean Si–O bond lengths do not increase significantly with temperature in any of the six pyroxenes. All remain within two standard deviations of those at room temperature (Table A–4). The largest increase observed was that in ureyite, 1.624 Å at 24°C to 1.629 Å at 600°C (an increase of 0.3 percent), whereas there was essentially no change

TABLE 2. Polyhedral Volumes

Mineral	Temperature (°C)	Volume (Å^3) of tetrahedron	Volume (Å^3) of M(1) octahedron	Volume (Å^3) of M(2) polyhedron
Spodumene	24	2.158	9.240	10.750
	300	2.162	9.320	10.846
	460	2.163	9.372	10.909
	760	2.165	9.457	11.023
Jadeite	24	2.183	9.373	24.581
	400	2.183	9.467	24.900
	600	2.186	9.528	25.088
	800	2.188	9.561	25.301
Acmite	24	2.201	10.869	26.295
	400	2.205	10.922	26.536
	600	2.209	11.001	26.774
	800	2.209	11.047	26.984
Ureyite	24	2.188	10.508	25.361
	400	2.196	10.602	25.699
	600	2.206	10.604	25.871
Diopside	24	2.221	11.848	25.760
	400	2.229	12.047	26.193
	700	2.228	12.206	26.576
	850	2.229	12.244	26.686
	1000	2.237	12.353	26.870
Hedenbergite	24	2.224	12.808	26.102
	400	2.224	12.946	26.468
	600	2.227	12.993	26.702
	800	2.225	13.092	26.886
	900	2.226	13.132	27.056
	1000	2.226	13.172	27.221

in hedenbergite from 24°C to 1000°C. Relative to bridging and non-bridging oxygens, a tendency may exist for the mean Si–O (br) lengths to increase at a slightly higher rate than the Si–O (nbr), but the changes are well within experimental errors.

As expected from the small changes in mean Si–O lengths, the volumes of the tetrahedra increase little with temperature for the six pyroxenes (Table 2). Mean thermal expansion coefficients for the mean Si–O distances and the tetrahedral volumes are listed in Table 3. The change in the shape of the tetrahedra with increasing temperature can be described by comparing the O–Si–O tetrahedral angles and the O–O distances of the room-temperature structure with those of the higher temperature structures for each mineral. In general, the tetrahedral angles O(1)–Si–O(3C2) and O(1)–Si–O(3C1) decrease in all six pyroxenes with increasing temperature, whereas O(1)–Si–O(2) and O(3C1)–Si–O(3C2) increase with the exception of diopside where O(1)–Si–O(2) is identical at room temperature and at 1000°C (Table A-6). The two remaining tetrahedral angles, O(2)–Si–O(3C1) and O(2)–Si–O(3C2), decrease in the sodic pyroxenes and increase in the calcic pyroxenes.

Because individual Si–O distances remain statistically identical with increasing temperature, it is important to examine the tetrahedral angles for trends which may help in understanding the nature of bonding within the tetrahedra. Brown and Gibbs (1970, Fig. 5, p. 595) have shown that in silicates which contain both bridging and non-bridging oxygens, the mean Si–O(br) distance depends in part upon the Si–O–Si angle, the shortest bonds usually being associated with the widest angles. This relation is valid for the room-temperature pyroxene structures [for the sodic pyroxenes, Si–O3–Si ~ 139° and Si–O(br) ~ 1.64Å and for the calcic pyroxenes Si–O3–Si ~ 136° and Si–O(br) ~ 1.68Å], but not for the individual minerals within the sodic or calcic groups, possibly because the Si–O–Si angles in the group may not be statistically different (range is ~ 0.5°). With increasing temperature, the Si–O–Si angle increases (a maximum of about 1.4° in both diopside and hedenbergite), and based on the conclusion of Brown and Gibbs (1970), we would expect the Si–O(br) bonds to decrease slightly. Examination of Table A-4 shows that the Si–O(br) bonds do not appear to decrease in any of the pyroxenes.

M(1) Octahedra

Mean *M*–O distances (Fig. 8) and volume of the *M*(1) octahedron (Fig. 9) both increase linearly

TABLE 3. Mean Thermal Expansion Coefficients (°C^{-1} × 10^5) for Individual, Mean *M*–O Distances and Polyhedral Volumes*

	Spodumene $\alpha_{24\text{-}760^\circ C}$	Jadeite $\alpha_{24\text{-}800^\circ C}$	Acmite $\alpha_{24\text{-}800^\circ C}$	Ureyite $\alpha_{24\text{-}600^\circ C}$	Diopside $\alpha_{24\text{-}1000^\circ C}$	Hedenbergite $\alpha_{24\text{-}1000^\circ C}$
Silicon tetrahedra						
Si-O(1)	0.379**	0.074	0.279	1.31	0.025	2.16
-O(2)	-0.180	0.142	--	1.14	-0.020	-0.158
-O(3C1)	0.157	0.064	0.447	-0.851	0.362	0.038
-O(3C2)	0.178	0.267	0.059	0.481	0.180	0.144
mean Si-O	0.160	0.156	0.182	0.529	0.099	0.026
tet. vol.	0.432	0.300	0.509	1.37	0.057	0.098
M(1) octahedron						
M(1)-O(1A1),(1B1)	1.79	1.79	1.67	1.33	2.08	1.94
-O(1A2),(1B2)	0.427	0.541	0.271	0.352	0.418	-0.298
-O(2C1),(2D1)	0.887	0.411	0.483	0.035	1.83	1.46
mean M(1)-O	1.06	0.947	0.781	0.633	1.44	1.05
M(1) vol.	3.21	2.65	2.16	1.69	4.25	2.91
M(2) polyhedron						
M(2)-O(1A1),(1B1)	2.58	1.67	1.98	1.63	1.71	1.49
-O(2C2),(2D2)	0.457	1.35	1.19	0.791	0.795	0.878
-O(3C1),(3D1)	2.81	0.854	1.14	0.913	0.958	0.415
-O(3C2),(3D2)	-1.74	1.32	0.793	1.66	3.00	3.47
mean M(2)-O	1.97	1.28	1.28	1.26	1.64	1.61
M(2) vol.	3.46	3.74	3.38	3.50	4.42	4.29

*Mean thermal expansion coefficients α are computed from the equation $\alpha_X = \frac{1}{X_{24}} \cdot \frac{X_T - X_{24}}{T-24}$, where the slope of the regression equation is used for the term $\frac{X_T - X_{24}}{T-24}$. See text of paper.

**For 0.379, read 0.379 x 10^{-5}C^{-1}.

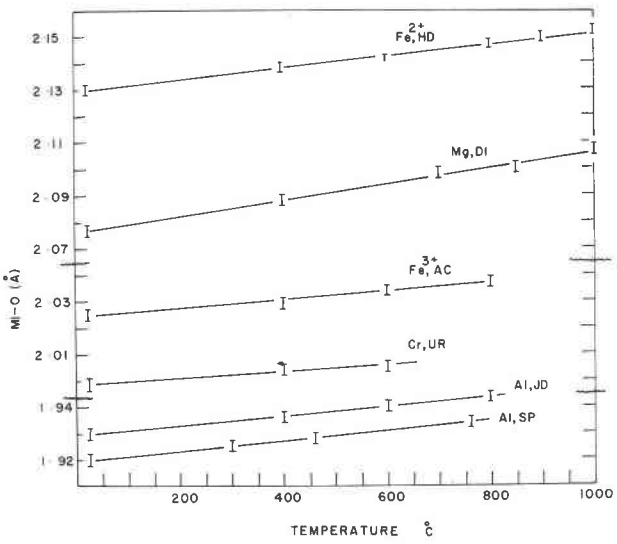

FIG. 8. Variation of mean $M(1)$-O interatomic distances with increasing temperature for six clinopyroxenes. (Abbreviations are the same as those in Figure 2.) Error bars represent ± 1 standard deviation.

with increasing temperature. The increase in mean $M(1)$–O bonds is almost an order of magnitude larger than that of the mean Si–O bonds and apparently reflects the lower strength of the M–O bond relative to the Si–O bonds. Ranking of the mean thermal expansion coefficients (Table 3) of mean M–O bond lengths results in the following sequence $Mg–O > Fe^{2+}–O > Al–O > Fe^{3+}–O > Cr^{3+}–O$.

If we examine the changes in individual $M(1)$–O bond lengths (Table A-7) with increasing temperature, we find that the $M(1)$–O(1A1), (1B1) bond has the highest mean thermal expansion coefficient in all six pyroxenes and the $M(1)$–O(1A2),(1B2) bond, which lies in a plane almost perpendicular to the b axis, has the lowest in four of the six pyroxenes. The changes in octahedral O–O distances (Table A-8) are very similar for the two calcic and three sodic pyroxenes. The main difference observed is a decrease in O(2C1)–O(2D1) in the sodic pyroxenes and an increase of this same distance in the calcic ones. The O–$M(1)$–O angles (Table A-9) change on the order of a few degrees, usually less, with increasing temperature.

M(2) Polyhedra

The $M(2)$ sites in both the calcic and sodic pyroxenes are 8-coordinated, whereas the Li in spodumene is 6-coordinated. Mean $M(2)$–O interatomic distances (Fig. 10) and polyhedral volumes (Fig. 11) increase linearly with increasing temperature. The magnitude of the changes in mean $M(2)$–O distances is approximately the same as that of the mean $M(1)$–O distances, *i.e.*, both are an order of magnitude larger than that of the silicate tetrahedra. The mean thermal expansion coefficients

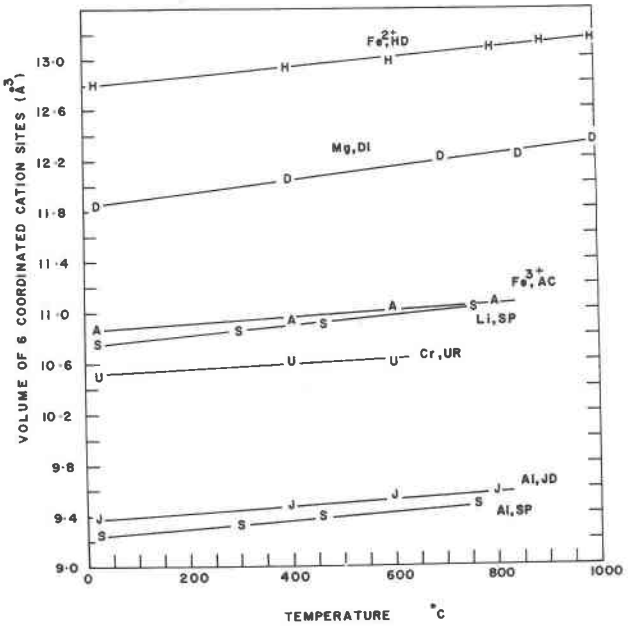

FIG. 9. Variation of octahedral volume with increasing temperature for six clinopyroxenes. (Abbreviations are the same as those in Figure 2.)

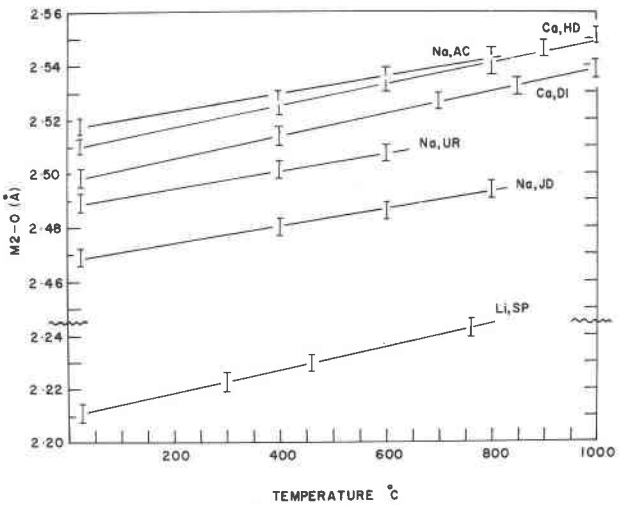

FIG. 10. Variation of mean $M(2)$-O interatomic distances with increasing temperature for six clinopyroxenes. (Abbreviations are the same as those in Figure 2.) Error bars represent ± 1 standard deviation.

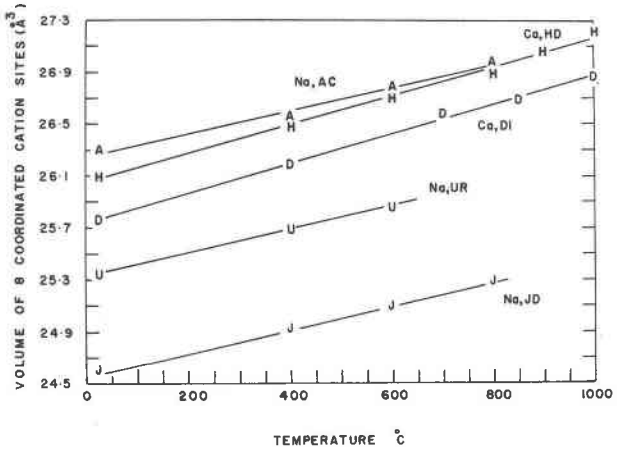

FIG. 11. Variation of $M(2)$ polyhedral volume with increasing temperature for five clinopyroxenes. The volume of the $M(2)$ polyhedron in spodumene is shown in Figure 9. (Abbreviations are the same as those in Figure 2.)

for the mean $M(2)$–O bonds (Table 3) are nearly identical for Na in the three sodic pyroxenes and for Ca in the two calcic pyroxenes. However, $\alpha_{M(2)\text{ volume}}$ varies somewhat from mineral to mineral within each series, probably as a result of the slightly different distortions. It is of interest to note that $\alpha_{\text{mean }M(2)\text{-O}}$ for Na in acmite, jadeite, and ureyite is less than that for Ca in diopside and hedenbergite.

Of the eight oxygens coordinating the $M(2)$ sites in the sodic and calcic pyroxenes, four are shared with the $M(1)$ octahedra and four with the silicate tetrahedral chains. The coordination polyhedra of these two pyroxene groups have different configurations at room temperature. The sodic pyroxene (Fig. 12a) have six short bonds (2.3–2.4Å) and two considerably longer (2.7–2.8Å), whereas the calcic pyroxenes (Fig. 12b) have four short bonds (~ 2.35Å) and four longer ones (2.55Å–2.7Å). In spodumene where the Li in the $M(2)$ is 6-coordinated, all bonds are short (2.1–2.5Å); the two next closest oxygens lie at a distance of 3.144Å and are well beyond the first neighbor cordination sphere. The $M(2)$–O(3C2),(3D2) interatomic distance is always the largest in the pyroxenes and it is these two oxygens which move in or out of $M(2)$ coordination sphere when coordination number of the $M(2)$ site changes.

Since the movements of the O(3) oxygens are intimately interconnected with the straightening of the tetrahedral chains, the changes that occur in the $M(2)$ coordination polyhedra with increasing temperature are complex. In spodumene the $M(2)$–O(3C2),(3D2) interatomic distance decreases significantly at higher temperatures (3.144Å at 24°C to 3.103Å at 760°C) although the O(3C2) and O(3D2) oxygens are still too distant to be considered as coordinating the lithium. This same interatomic distance increases considerably in both diopside (2.717Å to 2.797Å) and hedenbergite (2.720Å to 2.812Å) over the 1000°C interval studied, thus indicating that the Ca in $M(2)$ in both pyroxenes is becoming more nearly 6-coordinated. This result has important consequences in solid solution of the calcium-rich and calcium-poor pyroxenes where $M(2)$ is generally 6-coordinated. The increase in the $M(2)$–O(3C2),(3D2) distances in the sodic pyroxenes is almost an order of magnitude smaller than that in the calcic pyroxenes. The large increase in the $M(2)$–O(3C2),(3D2) bond in the

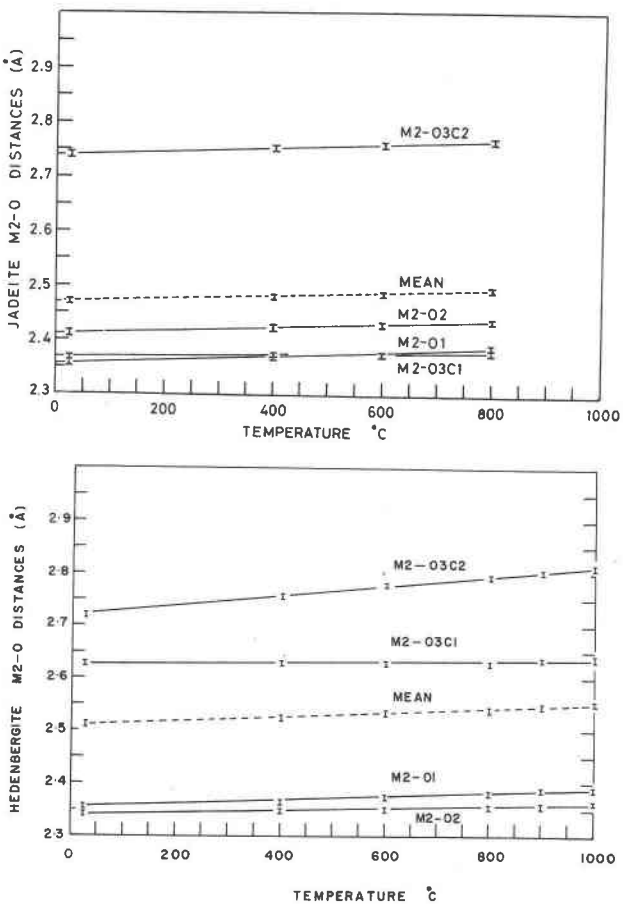

FIG. 12. (a) Variation in individual $M(2)$-O interatomic distances with increasing temperature in jadeite. (b) Variation in individual $M(2)$-O interatomic distances with increasing temperature in hedenbergite. Error bars represent ±3 standard deviations in both figures.

calcic proxenes results from a higher rate of tetrahedral chain straightening (Fig. 13) which in turn is due, at least in part, to the high rate of expansion of Fe^{2+} and Mg in the $M(1)$ sites. This effect is reflected in the increase in β angle for the calcic pyroxenes.

The relative movements of the $M(2)$ cations with increasing temperature has been determined from the ratio of the $M(2)$–O(1A1),(1B1) distance to the $M(2)$–O(3C1),(3D1) distance. With the exception of ureyite, the Ca and Na atoms move away from the octahedral strip.

Thermal Parameters

Isotropic Temperature Factors

In general, equivalent isotropic temperature factors, calculated using L. W. Finger's ERROR program and results from the anisotropic refinements, increase at the highest rate for 8-coordinated cations (Fig. 14) but at the lowest for 4-coordinated cations (Fig. 15). An exception is 6-coordinated Li in $M(2)$ in spodumene, for which the rate of increase was the highest observed. Because of the linear trend determined for B(Å²) for the Li atom, it does not

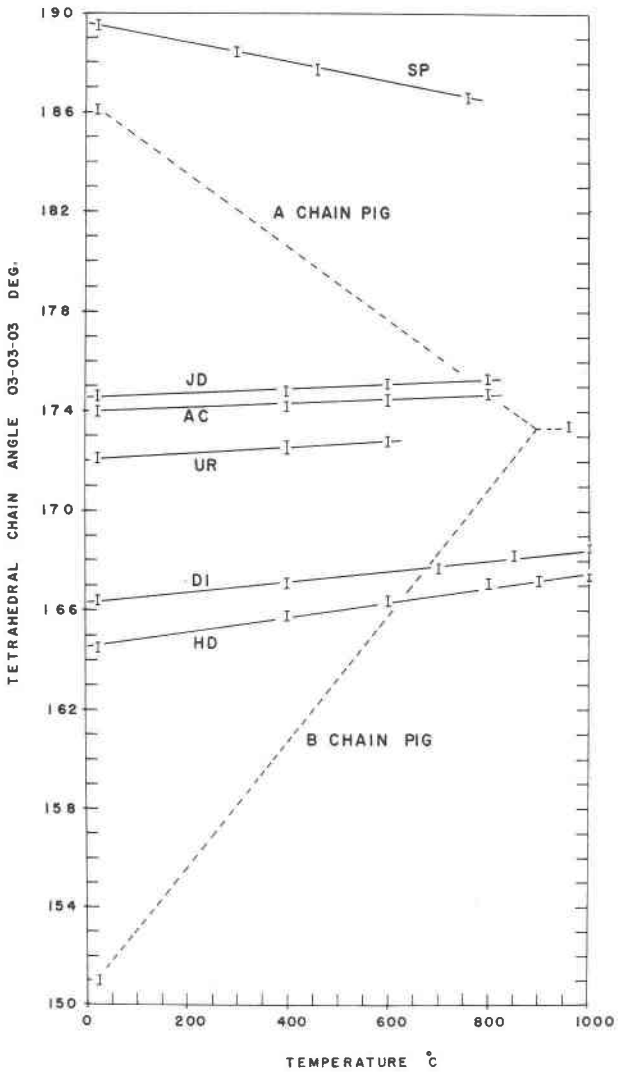

FIG. 13. Variation of the tetrahedral chain angle, O(3)–O(3)–O(3), with increasing temperature for the six clinopyroxenes of this study and the A and B chains in pigeonite (Brown *et al.*, 1972). (Abbreviations are the same as those in Figure 2.) Error bars represent ±1 standard deviation.

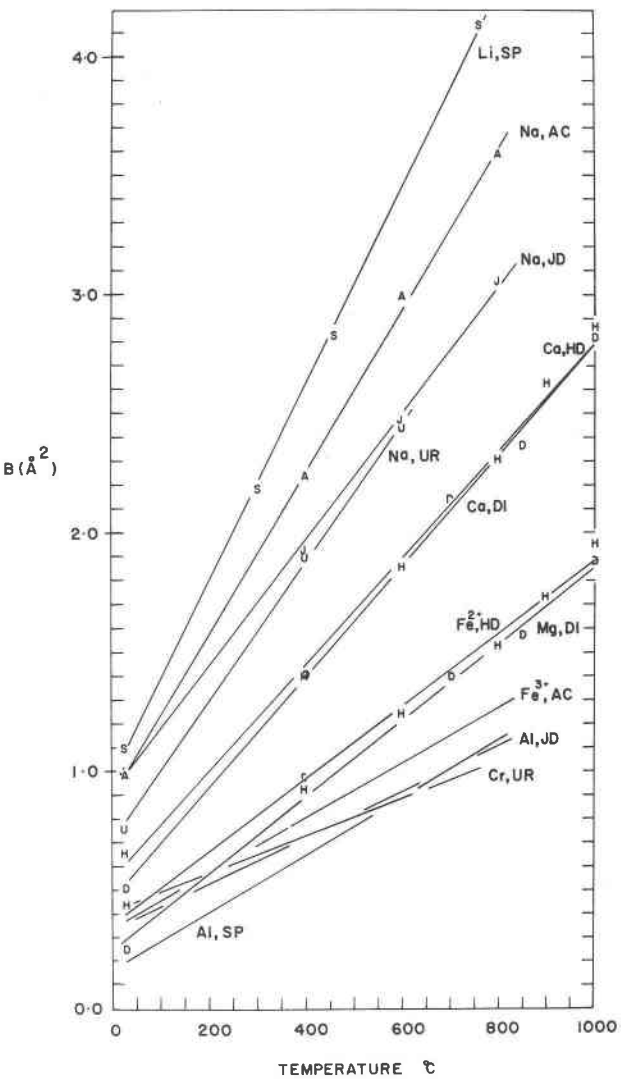

FIG. 14. Variation with increasing temperature of the equivalent isotropic temperature factors of 6- and 8-coordinated cations in six clinopyroxenes. (Abbreviations are the same as those in Figure 2.)

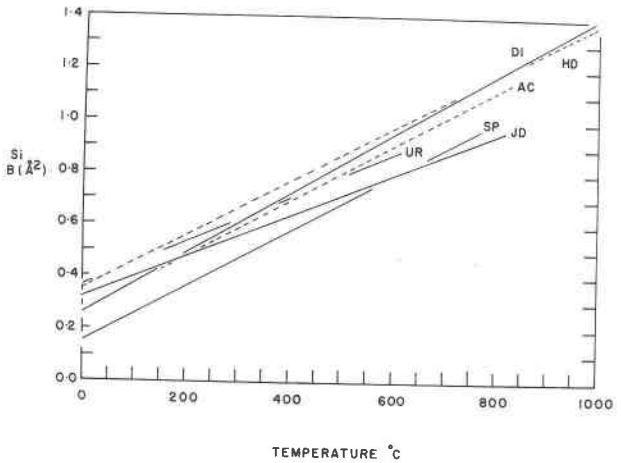

FIG. 15. Variation with increasing temperature of the equivalent isotropic temperature factors of 4-coordinated silicon atoms in six clinopyroxenes. (Abbreviations are the same as those in Figure 2.)

seem that a significant amount of Li could have been lost during the heating experiments. In general, the rate of increase in the isotropic temperature factors of the cations increases with increasing coordination number (hence increased M–O distances), decreasing charge on the cation (less electrostatic attraction), and increasing electro-positivity.

It is of interest to examine the relationship between mean bond length expansions and rate of increase of the isotropic temperature factors, since bond length expansions could reflect increased amplitude of vibration of the atoms. We have plotted dB/dT *vs* $\alpha_{\text{mean } M\text{-O}}$ rather than α_B *vs* $\alpha_{\text{mean } M\text{-O}}$ (Fig. 16) and our reasoning for this follows. The majority of the room-temperature structures were done by other workers, and although the refinements are quite good, we have found in our work that the isotropic temperature factors are extremely sensitive to data collection and refinement procedures. The positive trend in Figure 16 suggests that, in general, a positive correlation exists between bond length expansions and the increase in isotropic temperature factors, although *in detail* a direct correlation does not appear to exist. This is consistent with the observation that the isotropic temperature factor of silicon increases significantly with increasing temperature whereas the mean bond length appears to show little or no increase. This rate of increase, dB/dT, was determined to be as follows: Cr, 0.769; Si, 0.993; Al, 1.083; Fe^{3+}, 1.196; Fe^{2+}, 1.535; Mg, 1.619; Ca, 2.301; Na, 2.982; Li, 4.114 (all times 10^{-3}Å^2/°C). These figures reveal that $(dB/dT)_{Mg} > (dB/dT)_{Fe^{2+}} > (dB/dT)_{Fe^{3+}}$ and that Cr^{3+} has the lowest rate of increase with increasing temperature when compared to all atoms. Differences in dB/dT for the same atoms—for example, Al in spodumene and jadeite (Fig. 14)—may result in part from varying configurations of the sites in different structures and in part from different atomic species in $M(2)$—for example, Li in spodumene but Na in jadeite—with which $M(1)$ shares edges.

The rates of increase of the oxygen isotropic temperature factors lie roughly between those of the 6- and 8-coordinated cations, and their rate of increase can also be correlated with coordination number. With the exception of spodumene, the rate of increase for the 3-coordinated O(2) oxygen is greater than that for the 4-coordinated O(1) and O(3) oxygens. Although both O(1) and O(3) are coordinated by four cations in a very distorted tetrahedral arrangement, the four cations coordinating O(1) are closer (~ 2.4Å) than those cordinating O(3) (two > 2.58Å). Consequently, B(Å^2) for the apical O(1) oxygen has a lower rate of increase with temperature.

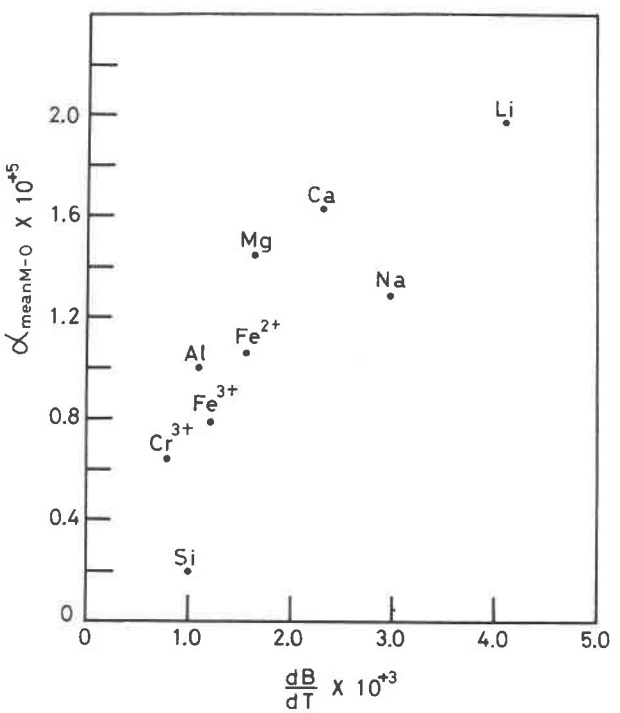

FIG. 16. Relationship between the rate of increase of equivalent isotropic temperature factors and mean thermal expansion coefficients of mean M-O interatomic distances.

Thermal Ellipsoids

Since the $M(1)$ and $M(2)$ cations in the $C2/c$ pyroxenes lie on a two-fold rotation axis, the orientations of their thermal ellipsoids are constrained to certain crystallographic directions. Symmetry requires that one of the three principal axes of the ellipsoid must lie parallel to the 2-fold axis (which is parallel to the b crystallographic axis) and the two remaining ellipsoid axes are therefore constrained to a plane at right angles to this direction. The pyroxenes included in this study are all highly ordered end members and, with the possible exception of Li in spodumene, we have assumed that positional disorder is at a minimum and that the *rms* displacements observed are mainly the result of thermal motion.

The thermal ellipsoids of atoms occupying the $M(1)$ site are not highly anisotropic and the orientation of the longest ellipsoid axes varies considerably from structure to structure. The Al atom in spodumene has an almost spherical vibration surface, whereas the Al in jadeite, Fe^{3+} in acmite, and Fe^{2+} atoms in hedenbergite are slightly triaxial. With increasing temperature, these ellipsoids maintain roughly the same shape but their *rms* amplitudes of vibration increase in all directions. The thermal ellipsoid of the Cr atom in ureyite becomes more prolate at high temperatures and that of the Mg atom in diopside changes from prolate to oblate. The atoms occupying the $M(2)$ site have vibration ellipsoids which are highly anisotropic (Table A-11). The Na and Ca atoms can be described as having prolate triaxial ellipsoids; that is, the three axes are unequal, but two are similar in length and the third is much longer. The vibration ellipsoid of the Li atom in spodumene is almost spherical at room temperature, but becomes more oblate at high temperatures. Ellipsoids characterizing pure thermal motion are prolate with the long axis perpendicular to b, whereas structures in which positional disorder is also a factor have oblate ellipsoids whose short axis is perpendicular to b. The lengthening of the ellipsoid axis parallel to b in the latter instance is the result of different cations occupying slightly different positions along the b axis. This effect has been pointed out by Takeda (1972) and is discussed for amphiboles by Sueno *et al* (1973). With increasing temperature, the lengths of the 3 ellipsoid axes increase, the long axis at a slightly higher rate in most of the minerals. The orientation of the $M(2)$ ellipsoids appears to be strongly controlled by configuration of the site. The orientation of the long axis of the vibration ellipsoids is very similar for all the pyroxenes and changes very little with increasing temperature. To emphasize the similarity in orientation, the angular relationships of the long axes with the crystallographic axes as 400°C are listed below:

	angle to a	angle to b	angle to c
Na (jadeite)	160°	90°	52°
Na (acmite)	159	90	52
Na (ureyite)	154	90	47
Ca (diopside)	155	90	49
Ca (hedenbergite)	158	90	53

The shortest axis of the ellipsoid is usually perpendicular to the plane containing the long ellipsoid axis and the b crystallographic axis. The short axis of the oblate spheroid of Li is oriented similarly.

The silicon and oxygen atoms occupy general positions in the pyroxene structure and thus neither the orientation nor the shape of their vibration ellipsoids are constrained in any manner.[7] The silicon atoms have triaxial vibration ellipsoids which are not markedly anisotropic and whose orientation varies from structure to structure. In general, the oxygen thermal ellipsoids are triaxial with the longest axis lying approximately perpendicular to the associated Si-O bond. For example, the long axes of the O(1) and O(2) vibration ellipsoids are oriented at high angles to the Si-O(1) and Si-O(2) bonds, respectively, and the O(3) oxygens, each of which are bonded to two silicon atoms, have vibration ellipsoids whose long axis is also at high angles to the Si-O-Si plane.

Discussion

Differential Polyhedral Expansion

One of the most important aspects of thermal expansion in pyroxenes is the concept of differential polyhedral expansion, since it may be possible to correlate the relative sequence of rates of expansion or mean thermal expansion coefficients (Table 4) with

[7] It must be emphasized that the shapes and orientations of the thermal ellipsoids listed in Table A-11 were calculated for atoms occupying the positions listed in Table A-3. Application of this data to atoms outside the asymmetric unit is correct only after the appropriate symmetry transformations have been applied.

TABLE 4. Mean Thermal Expansion Coefficients ($°C^{-1} \times 10^5$) and Rate of Increase of Mean *M*–O Distances ($Å/°C \times 10^5$).

Bond	Coordination Number	$\alpha_{\text{mean M-O}}$	d(M-O)/dT
Si-O	4	0.192[a]	0.312[b]
Cr-O	6	0.633	1.264
Fe^{3+}-O	6	0.781	1.581
Al-O	6	1.002	1.111
Fe^{2+}-O	6	1.048	2.231
Mg-O	6	1.442	2.995
Na-O	8	1.276	3.180
Ca-O	8	1.627	4.075
Li-O	6	1.967	4.349

[a]For 0.192, read 0.192×10^{-5} C^{-1}.

[b]For 0.312, read 0.312×10^{-5} Å/°C.

relative bond strengths of the various *M*–O bonds. In general, the smaller values of both $\alpha_{\text{mean } M-O}$ and $d(M\text{–O})/d\text{T}$ are associated with (1) decreased coordination number of the cations, (2) more highly charged cations, and (3) more electronegative cations. The correlation with coordination number can be understood in terms of the inverse relationship between bond strength and interatomic distance (Badger, 1935). The type of bond is also important since mean thermal expansion coefficients for compounds such as alkali halides are much higher than those for compounds such as diamond where the type of bonding is significantly different. The relation with cation charge is consistent with spectral data which show that the frequencies for the symmetric modes of vibration decrease with decreasing charge on the cation. Spectra for various polyhedra important in silicate structures have been calculated by Alekhina and Akhmanova (1971) using the structure of forsterite as a model. Frequencies determined for the totally symmetric stretch of groups with $T_d(\bar{4}3m)$ symmetry (SiO_4) and $O_h(4/m\bar{3}2/m)$ symmetry ($Mg^{2+}O_6$, $Fe^{2+}O_6$, $Fe^{3+}O_6$, $Al^{3+}O_6$, $Cr^{3+}O_6$) have been substituted in the equation $k = 4\nu^2\pi^2\mu c^2$, where ν is frequency, μ is reduced mass, and c is the velocity of light. The resulting force constants show an inverse relationship with $\alpha_{\text{mean } M-O}$ values (Fig. 17).

It has been generally stated that thermal stability, as characterized by melting temperature or temperature of dissociation, will be controlled in part by the weakest bonds (Urisov, 1967). Experimental studies of Fe^{2+}–Mg silicate systems reveal that Fe-bearing silicates usually have lower thermal stabilities than their Mg-analogues, thus indicating that Fe^{2+}–O bonds may be weaker. In this study, however, the mean Mg–O bond in diopside exhibits both a higher rate of increase and a higher mean thermal expansion coefficient than the mean Fe^{2+}–O bond in hedenbergite. Our expansion data for diopside ($\alpha_V = 3.33\text{x}10^{-5}$ $°C^{-1}$) and hedenbergite ($\alpha_V = 2.98\text{x}10^{-5}$ $°C^{-1}$) are also consistent with expansion data in other Fe and Mg end member silicates and oxides (B. Skinner, *in* Clark, 1966). For example,

$\alpha_V = 2.64 \times 10^{-5}C^{-1}$ for fayalite
$\alpha_V = 3.86 \times 10^{-5}C^{-1}$ for forsterite at 1000°C

$\alpha_V = 2.38 \times 10^{-5}C^{-1}$ for almandite ($Fe^{2+}Al$)
$\alpha_V = 2.51 \times 10^{-5}C^{-1}$ for pyrope ($Mg^{2+}Al$) at 800°C

$\alpha_V = 3.50 \times 10^{-5}C^{-1}$ for FeO
$\alpha_V = 3.75 \times 10^{-5}C^{-1}$ for MgO at 600°C

Mechanisms of Thermal Expansion

An obvious problem that arises as a result of the differential mean *M*–O expansions is how the silicate chains and octahedral layers accommodate these expansions with increasing temperature. Mechanisms for accomplishing this include: (1) extension of the silicate tetrahedral chains, (2) distortion of the sili-

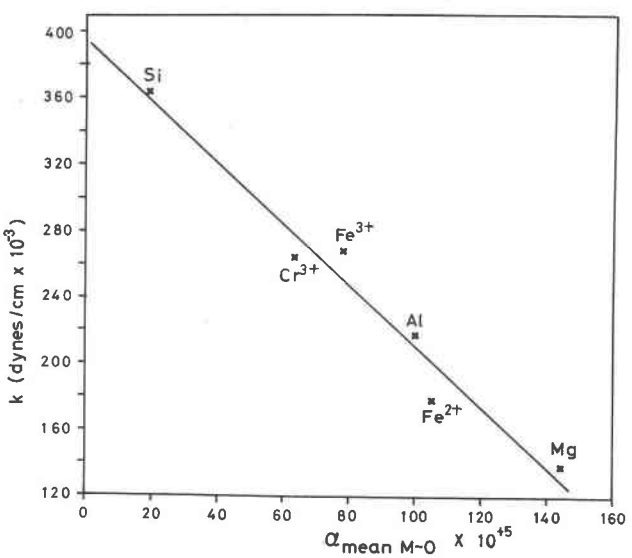

FIG. 17. Relationship between force constants and mean thermal expansion coefficients of mean *M*-O interatomic distances. See text of paper for explanation.

cate tetrahedra, and (3) an increase in out-of-plane tilting, that is, tilting the tetrahedra as a result of movement of the O(2) atom farther from the *bc* plane which contains the O(3) atoms.[8] Extension of the tetrahedral chains in the *c* direction (Fig. 13) involves a rotation of 2–3 degrees; and over the temperature ranges investigated, the increase is linear. The tetrahedral chains in spodumene, which exhibit S-rotations (Papike *et al,* 1973), also straighten with increasing temperature. The relatively small changes in the O3–O3–O3 angles of the pyroxenes included in this study contrasts strongly with those that occur in pigeonite over comparable temperature intervals (Brown *et al,* 1972). Structural accommodation is also aided by small increases in the out-of-plane tilting (~0.5° for diopside and ureyite) and by slight distortions involving an increase in the O(3C1)–O(3C2) interatomic distances. Change in distortion of the silicate tetrahedra appears to be a relatively minor mechanism in thermal expansion in pyroxenes because the tetrahedral angle variance, which gives a quantitative measure of distortion (Robinson, Gibbs, and Ribbe, 1971), varies considerably more from one pyroxene to another than it does for each pyroxene with increasing temperature (Table 5).

The volume of the space between the cation polyhedra, determined by subtracting the volumes of all polyhedra in a unit cell from the cell volume, increases linearly with temperature in all six pyroxenes (Fig. 18). At room temperature the polyhedra in the sodic and calcic pyroxenes account for 38–39 percent of the cell volume but with increasing temperature, expansion of the polyhedra account for 43–50 percent of the increase in cell volumes. In spodumene they occupy 25 percent of the cell volume at room temperature, but at high temperatures they account for 32 percent of the increase in cell volume. Thus, it appears that the polyhedra expand partially at the expense of the interpolyhedral space (Table 1).

In summary, the phenomena of thermal expansion in pyroxenes can be attributed to expansion of the cation-containing polyhedra with concomitant expansion of the voids between the cation polyhedra (Table 1), and rotation of the fairly rigid tetrahedra. Isotropic temperature factors of the oxygen atoms and the increase in the Si–O–Si angles provide supporting evidence that the bridging oxygens act as pivotal points during thermal expansion.

[8] A study investigating the relative importance of these three mechanisms is in progress.

TABLE 5. Tetrahedral Angle Variance for Silicate Tetrahedra in Six Clinopyroxenes

Structure	$\sigma^2_{\theta(tet)}$ *	Structure	$\sigma^2_{\theta(tet)}$ *
Spodumene		Jadeite	
24°C	18.21	24°C	22.89
300°C	18.34	400°C	24.24
460°C	18.58	600°C	24.09
760°C	18.84	800°C	24.58
Acmite		Ureyite	
24°C	13.77	24°C	15.79
400°C	15.30	400°C	16.78
600°C	15.44	600°C	18.22
800°C	16.38		
Diopside		Hedenbergite	
24°C	28.44	24°C	24.97
400°C	27.93	400°C	24.63
700°C	26.57	600°C	24.72
850°C	27.85	800°C	25.05
1000°C	27.78	900°C	24.74
		1000°C	24.56

* $\sigma^2_{\theta(tet)} = \sum_{i=1}^{6} (\theta_i - 109.47^\circ)^2/5.$

Cell Parameters

With the exception of spodumene, mean thermal expansion coefficients for the cell parameters (Table 1) decrease in the order $\alpha_b > \alpha_a > \alpha_c$. The apparently anomalous behavior of the *a* axis in spodumene has been discussed in a previous section and its mean thermal expansion coefficient is comparable with that of the d_{100} directions in the other five pyroxenes. The low rate of increase for *c* may be related to a "clamping" or "restraining" effect of the relatively inert tetrahedral chains. The high rate of expansion for the *b* direction relative to the *a* can be explained by a consideration of "paths" through the structure in these directions. Along the *b* direction a path through the structure can be defined which involves only 6- and 8-coordinated sites which show a relatively large thermal expansion rate. In the *a* direction, however, the "path" traverses both octahedral and tetrahedral layers, and since expansion of the silicate tetrahedra is negligible, a relatively lower thermal expansion is exhibited. Comparison of mean thermal expansion coefficients of individual bonds also shows that bonds in $M(1)$ and $M(2)$ polyhedra increase at a higher rate in the *b* direction than in

the *a* or *c* directions. In all six pyroxenes, the $M(1)$–O(1A2),(1B2) bonds which have large bond-length components in both the *a* and *c* directions and almost none in the *b* direction, exhibit low mean thermal expansion coefficients.

Examination of the individual plots of each cell parameter shows that the relative expansions in the *a*, d_{100} and *c* directions in the six pyroxenes cannot be simply explained by a consideration of the mean thermal expansion coefficients given in Table 4, and additional factors, such as distortion, must be taken into account. Mean thermal expansion coefficients for the *b* cell dimension do expand largely as predicted from a consideration of $\alpha_{\text{mean } M\text{-O}}$. The larger values of the mean thermal expansion coefficients for the *b* direction in the two calcic pyroxenes may be a result of the combination of the relatively large $\alpha_{\text{mean } M\text{-O}}$ values of the Ca–O, Mg–O, and Fe^{2+}–O bonds.

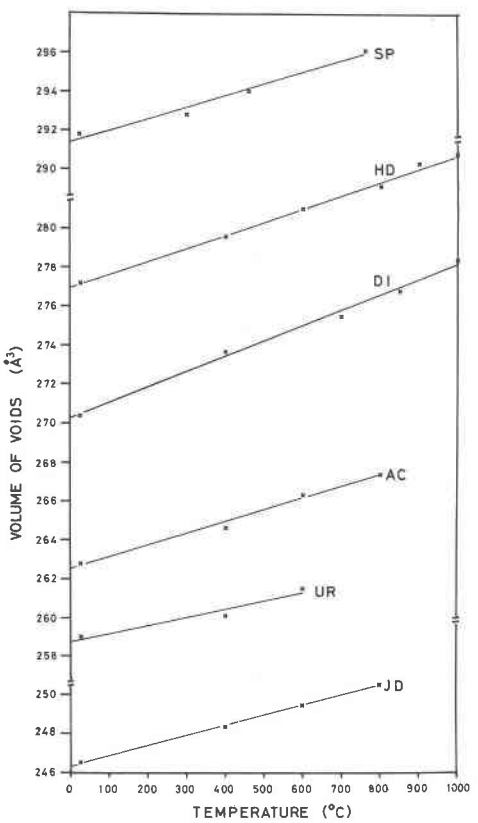

FIG. 18. Variation, with increasing temperature, of the volume of the space between the cation polyhedra in the unit cells of six clinopyroxenes. The volume is determined by subtracting the volumes of all polyhedra in a unit cell from the unit cell volume. (Abbreviations are the same as those in Figure 2.)

As has been noted in previous sections, the β angle of each of the six pyroxenes behaves uniquely with increasing temperature. In the sodic pyroxenes, it decreases or remains approximately the same, whereas in the calcic pyroxenes, it increases nonlinearly. The calcic pyroxenes with smaller β angles and more kinked tetrahedral chains have shorter $M(2)$–O(3C2),(3D2) distances (~2.7Å) than in the sodic pyroxenes (~2.8Å). As a result, with increasing temperature and concomitant straightening of the tetrahedral chains, the calcic pyroxenes can accommodate an increase in the β angle and still maintain the 8-fold coordination. The sodic pyroxenes would not be able to maintain 8-fold coordination, if both O(3)–O(3)–O(3) and β increased, and thus the β angles either decrease (acmite and ureyite) or remain constant (jadeite). The $M(2)$–O(3C2),(3D2) bond in jadeite is significantly shorter than that in either acmite or ureyite, but not as short as those in diopside and hedenbergite; therefore with increasing temperature [and increasing O(3)–O(3)–O(3) angle] the 8-fold coordination can be maintained with little change in the β angle.

Mean thermal expansion coefficients for the unit cell volumes increase in the same sequence as the $\alpha_{\text{mean } M\text{-O}}$ values of the $M(1)$ and $M(2)$ sites (Table 3). This is as expected since the $\alpha_{\text{mean } M\text{-O}}$ values merely represent the average increase in *M*–O distances in all directions in the pyroxene structure.

Implications with Respect to Solid Solution Between Pigeonite and Augite

It is now known that significant differences exist between the $M(2)$ sites in high-calcium and low-calcium pyroxenes and between the analogous $M(4)$ sites in high-calcium and low-calcium amphiboles. It has also been concluded that these differences are largely responsible for the limited miscibility between the high-calcium and low-calcium varieties of these mineral groups (Papike, Ross, and Clark, 1969; Takeda, 1972). Takeda (1972) has discussed the changes that take place in quenched solid-solutions of low-calcium and high-calcium pyroxenes. He showed that when (Mg,Fe^{2+}) atoms are added to calcium-rich pyroxenes, the $M(2)$–O(3) bonds increase whereas the $M(2)$–O(1),O(2) bonds decrease. In addition, he demonstrated that when calcium is added to (Fe,Mg) pyroxenes, the $M(2)$–O(1), $M(2)$–O(2) and $M(2)$–O(3) bonds all increase. This increase in $M(2)$–O(3) bonds from either side of the solid-solution series leads to a

highly unsymmetric and unstable distribution of oxygens around the $M(2)$ cation. Thus, these observations are consistent with a large miscibility gap between high-calcium and low-calcium pyroxenes at low temperatures. However, we do know that considerable solid solution between these end-member types occurs at high temperatures. It is therefore, necessary to compare the high-temperature calcic and (Fe^{2+},Mg)-pyroxene structures. We now have the data to begin these comparisons with the high-temperature pigeonite data (Brown *et al,* 1972) and high-temperature diopside and hedenbergite data (reported here). Tables 6 and 7 show a comparison of the $M(2)$ sites of pigeonite, diopside, and hedenbergite at room, as well as high, temperature. These tables show about equal differences between the pigeonite $M(2)$–O distances and the averaged diopside, hedenbergite $M(2)$–O distances at both room temperature and high temperature. Therefore, the increased solid solution between these phases at high temperature cannot be explained by the fact that the sites become more similar through the increase of M–O distances, as has been previously suggested. What then is the reason for the significant increase in solid solution between pigeonite and augite with temperature? The answer appears to be in the coordination of the $M(2)$ cations in pigeonite at high temperature in space group $C2/c$ compared to that at low temperature in space group $P2_1/c$. In the transition from low to high pigeonite (Brown *et al,* 1972), the B tetrahedral chain undergoes significant extension and becomes equivalent to the A tetrahedral chain at the transition temperature. This chain straightening also causes a significant change in the primary coordination of the $M(2)$ cation. During the transition, one O(3) atom moves out and a different one moves into the coordination sphere of the $M(2)$ cation. Thus, although essentially six-coordinated in both room and high temperature, the nature of this six-coordinated $M(2)$ site changes significantly. These comparisons are discussed in detail by Brown *et al* (1972) and Papike *et al* (1973). An important aspect is that the $M(2)$ site in the high-temperature pigeonite structure (when the tetrahedral chains are relatively extended) can be readily transformed into an eight-coordinated site similar to that of diopside and hedenbergite by simple tetrahedral chain displacement. When Ca replaces (Mg, Fe^{2+}) in pigeonite at high temperature, the tetrahedral chains displace relative to each other so that two additional oxygens are brought into the coordination sphere. This is documented below.

	Pigeonite (960°C)	Hedenbergite, Diopside (1000°C)
M(2)–O(1)	2.176 (Å)	2.394 (Å)
M(2)–O(2)	2.081	2.366
M(2)–O(3)	2.656	2.612
M(2)–O(3)	3.173	2.804

Thus, with this tetrahedral chain displacement going from pigeonite to (diopside, hedenbergite) at high temperature, the $M(2)$–O(1) and $M(2)$–O(2) bonds become longer while the $M(2)$–O(3) and $M(2)$–O(3) bonds become shorter. This chain displacement is reflected in a rather large change in the β angle from 109.4° in pigeonite to 105.6° in diopside, hedenbergite. Therefore, it appears that as pigeonite is raised to higher temperatures, its $M(2)$ site and tetrahedral chain configuration change in such a manner that calcium can be accepted more readily

TABLE 6. Comparisons of $M(2)$–O Distances (Å) in Pigeonite and (Diopside + Hedenbergite) at Room and High Temperature

	Pigeonite*		Average, diopside+hedenbergite		Δ** (Å)	
	24°C	960°C	24°C	1000°C	24°C	High Temperature
M2-O1	2.154	2.176	2.358	2.394	+0.204	+0.218
M2-O2	2.053	2.081	2.347	2.366	+0.294	+0.285
M2-O3	2.866	2.914	2.655	2.708	-0.211	-0.206

*Pigeonite data from Brown et al (1972).

**Δ is the difference between the average diopside + hedenbergite M(2)-O distances and comparable distances in pigeonite.

TABLE 7. Comparison of Pigeonite, Diopside, and Hedenbergite $M(2)$–O Distances at Room and High Temperature

Bond	Distance (Å)	Bond	Distance (Å)
	Pigeonite		
	24°C ($P2_1/c$)		960°C ($C2/c$)
M2-O1A*	2.168	M2-O1	2.176
M2-O1B	2.140	M2-O1	2.176
M2-O2A	2.071	M2-O2	2.081
M2-O2B	2.035	M2-O2	2.081
M2-O3A	2.460	M2-O3	2.656
M2-O3B	2.663	M2-O3	3.173
M2-O3A'	3.407	M2-O3	3.173
M2-O3B'	2.935	M2-O3	2.656

	Diopside ($C2/c$)		Hedenbergite ($C2/c$)	
	24°C	1000°C	24°C	1000°C
M2-O(1A1),(1B1)	2.360	2.399	2.355	2.388
M2-O(2C2),(2D2)	2.353	2.370	2.341	2.363
M2-O(3C1),(3D1)	2.561	2.586	2.627	2.639
M2-O(3C2),(3D2)	2.712	2.797	2.720	2.812

*Data and nomenclature from Brown et al (1972).

into solid solution. In addition, it is interesting to note that diopside and hedenbergite are not passive in this regard but also change so that (Fe^{2+},Mg) can be accepted into solid solution. This is indicated in that their $M(2)$ sites are becoming more six-coordinated, as discussed above and indicated in Figure 12b. In conclusion, it is apparent that to understand the true atomistic model for solid solution between pigeonite and augite, data for the high-temperature structures is an absolute necessity.

Conclusions

1. With increasing temperature, the increase in mean Si–O interatomic distances of the six pyroxenes included in this study are not statistically significant. The largest change observed was that in ureyite, 1.624Å at 24°C to 1.629Å at 600°C.
2. Mean M–O distances and polyhedral volumes of both $M(1)$ and $M(2)$ sites increase regularly with increasing temperature. Rates of expansion for both sites are an order of magnitude greater than that of the tetrahedral sites.
3. Mean thermal expansion coefficients for mean M–O bonds increase in the following order: Si–O < Cr–O < Fe^{3+}–O < Al–O < Fe^{2+}–O < Na–O < Mg–O < Ca–O < Li–O. It may be possible to correlate this sequence with relative bond strengths.
4. As a result of differential thermal expansion of the mean M–O bonds, there is a structural misfit between the tetrahedral chains and the octahedral layers. Accommodation is accomplished by extension of the silicate tetrahedral chains, distortion of the tetrahedra, and out-of-plane tilting.
5. Rotation of the tetrahedra in the silicate chains in the $C2/c$ pyroxenes is on the order of a few degrees over the temperature intervals investigated.
6. Thermal expansion in pyroxenes can be attributed to expansion of the cation-containing polyhedra with concomitant expansion of the voids between the cation polyhedra, and rotation of the fairly rigid tetrahedra about the bridging oxygen atoms.
7. Except for β, the unit cell parameters of the six end-member pyroxenes included in this study increase linearly over the temperature intervals investigated.
8. Mean thermal expansion coefficients for the cell parameters generally decrease in the order $\alpha_b > \alpha_a > \alpha_c$. The greater expansion in the b direction can be explained by consideration of "paths" through the structure since a path parallel to a must traverse the fairly inert tetrahedral layer whereas a traverse parallel to b does not. Expansion in the c direction may be restrained by the relatively inert tetrahedral chains.
9. Mean thermal expansion coefficients are, in general, higher for the cell parameters of the calcic pyroxenes and are probably the result of the relatively high $\alpha_{\text{mean } M\text{-O}}$ values of the Ca–O, Mg–O and Fe^{2+}–O bonds.
10. In general, the equivalent isotropic temperature factors of the 4-coordinated cations increase at the lowest rate, whereas those of the 8-coordinated cations increase the fastest. The rate of increase in $B(Å^2)$, Cr < Si < Al < Fe^{3+} < Fe^{2+} < Mg < Ca < Na < Li, generally agrees with the rate of increase in mean M–O interatomic distances.
11. Oxygen isotropic temperature factors lie between those for the 6- and 8-coordinated cation sites. With one exception, their rate of increase is greater for the 3-coordinated O(2) oxygen than for the 4-coordinated O(1) and O(3) oxygens.
12. The thermal ellipsoids of atoms occupying the $M(2)$ sites are the most anisotropic atoms in the structures. The vibration ellipsoids for Ca and Na can be described as prolate triaxial ellipsoids whereas that for Li approximates an oblate spheroid. The orientation of the long axis of the ellipsoids is almost identical from pyroxene to pyroxene and, with increasing temperature, the orientations change very little. The main change with temperature is an increase in the size of the ellipsoids.

Acknowledgments

This research was supported by National Science Foundation Grant No. GA-12973. D. H. Lindsley is gratefully acknowledged for synthesizing the hedenbergite crystals. Thanks are also due L. Bence and S. King for typing the manuscript and P. Papike for helping compile the tables.

TABLE A-1. Data Collection Information for Six Clinopyroxenes

Mineral	Temperature (°C)	Number of reflections used in refinement	Isotropic R[a]	Isotropic wtd. R[b]	Anisotropic R	Anisotropic wtd. R
Spodumene	300	656	0.042	0.045	0.023	0.029
	460	652	0.049	0.055	0.026	0.035
	760	649	0.060	0.063	0.027	0.032
Jadeite	24	647	0.036	0.036	0.030	0.032
	400	661	0.057	0.057	0.034	0.036
	600	664	0.054	0.052	0.037	0.039
	800	659	0.067	0.064	0.049	0.049
Acmite	400	715	0.053	0.051	0.030	0.032
	600	724	0.060	0.057	0.032	0.034
	800	713	0.065	0.062	0.034	0.035
Ureyite	400	667	0.100	0.095	0.072	0.074
	600	651	0.099	0.097	0.077	0.078
Diopside	400	733	0.075	0.072	0.038	0.042
	700	721	0.082	0.075	0.039	0.039
	850	696	0.089	0.082	0.031	0.031
	1000	696	0.122	0.116	0.041	0.043
Hedenbergite	24	741	0.030	0.032	0.022	0.025
	400	747	0.052	0.051	0.027	0.029
	600	725	0.064	0.062	0.028	0.030
	800	734	0.078	0.074	0.032	0.033
	900	731	0.085	0.079	0.034	0.035
	1000	709	0.092	0.088	0.042	0.044

[a] $R = \Sigma||F_o| - |F_c||/\Sigma|F_o|$.

[b] wtd. $R = [\Sigma w(|F_o| - |F_c|)^2/\Sigma w|F_o|^2]^{\frac{1}{2}}$.

TABLE A-2. Unit Cell Parameters of Six Clinopyroxenes

Mineral	Temperature (°C)	a (Å)	b (Å)	c (Å)	β (°)	V (Å³)
Spodumene	24	9.463(1)[a]	8.392(1)	5.218(1)	110.15(1)	389.0(1)
	300	9.468(1)	8.412(1)	5.224(1)	110.05(1)	390.8(1)
	460	9.473(2)	8.430(1)	5.229(1)	109.99(1)	392.4(1)
	760	9.489(1)	8.460(1)	5.236(1)	109.88(1)	395.3(1)
Jadeite	24	9.423(1)	8.564(1)	5.223(1)	107.56(1)	401.8(1)
	400	9.450(2)	8.594(1)	5.233(1)	107.57(1)	405.2(1)
	600	9.469(2)	8.614(1)	5.240(1)	107.57(1)	407.4(2)
	800	9.483(1)	8.630(1)	5.2490(4)	107.59(1)	409.5(1)
Acmite	24[b]	9.658(2)	8.795(2)	5.294(1)	107.42(2)	429.1(1)
	400	9.677(1)	8.829(1)	5.298(1)	107.33(1)	432.1(1)
	600	9.699(1)	8.855(1)	5.307(1)	107.32(1)	435.1(1)
	800	9.711(1)	8.876(1)	5.312(1)	107.29(1)	437.2(1)
Ureyite	24	9.579(2)	8.722(1)	5.267(1)	107.37(1)	420.0(2)
	400	9.597(1)	8.751(1)	5.274(1)	107.29(1)	422.9(1)
	600	9.612(1)	8.770(1)	5.279(1)	107.25(1)	425.0(1)
Diopside	24[b]	9.746(4)	8.899(5)	5.251(6)	105.63(6)	438.6(3)
	400	9.776(1)	8.979(1)	5.267(1)	105.94(1)	444.5(1)
	700	9.799(1)	9.029(1)	5.274(1)	106.00(1)	448.5(1)
	850	9.806(1)	9.050(1)	5.280(1)	106.00(1)	450.4(1)
	1000	9.822(4)	9.081(1)	5.285(3)	105.98(3)	453.2(5)
Hedenbergite	24	9.845(1)	9.024(1)	5.245(1)	104.74(1)	450.6(1)
	400	9.870(1)	9.077(1)	5.258(1)	105.01(1)	455.0(1)
	600	9.884(1)	9.110(1)	5.264(1)	105.11(1)	457.6(1)
	800	9.897(1)	9.138(1)	5.269(1)	105.17(1)	459.9(2)
	900	9.906(1)	9.164(1)	5.273(1)	105.22(1)	461.9(1)
	1000	9.916(1)	9.179(1)	5.276(1)	105.28(1)	463.2(1)

[a] Errors in parentheses are 1 standard deviation.

[b] Cell parameters from Clark et al (1969).

TABLE A-3. Final Positional Parameters and Equivalent Isotropic Temperature Factors (Å²) for Six Clinopyroxenes

Atom	Parameter	Spodumene 24°C[a]	Spodumene 300°C	Spodumene 460°C	Spodumene 760°C	Jadeite 24°C	Jadeite 400°C	Jadeite 600°C	Jadeite 800°C	Acmite 24°C[a]	Acmite 400°C	Acmite 600°C	Acmite 800°C
O(1)	x	0.1099(2)[b]	0.1101(1)	0.1104(1)	0.1105(1)	0.1092(2)	0.1096(2)	0.1097(2)	0.1098(2)	0.1141(2)	0.1141(2)	0.1142(2)	0.1146(2)
	y	0.0823(2)	0.0819(1)	0.0815(2)	0.0810(2)	0.0760(2)	0.0756(2)	0.0756(2)	0.0751(3)	0.0784(2)	0.0778(2)	0.0775(2)	0.0771(2)
	z	0.1402(3)	0.1397(2)	0.1394(3)	0.1383(3)	0.1285(3)	0.1279(3)	0.1278(3)	0.1274(4)	0.1380(4)	0.1368(3)	0.1364(4)	0.1356(4)
	B	0.24(2)	0.67(2)	0.83(2)	1.21(2)	0.45(2)	0.80(2)	1.01(3)	1.23(4)	0.39(2)	0.93(3)	1.20(3)	1.48(3)
O(2)	x	0.3646(2)	0.3649(1)	0.3650(2)	0.3652(2)	0.3611(2)	0.3612(2)	0.3613(2)	0.3614(3)	0.3582(2)	0.3586(2)	0.3587(2)	0.3588(2)
	y	0.2673(2)	0.2662(1)	0.2656(2)	0.2644(2)	0.2633(2)	0.2622(2)	0.2615(2)	0.2611(3)	0.2558(2)	0.2545(2)	0.2537(2)	0.2532(2)
	z	0.3009(3)	0.3012(3)	0.3014(3)	0.3018(3)	0.2932(3)	0.2918(3)	0.2903(4)	0.2894(5)	0.3001(4)	0.2989(4)	0.2975(4)	0.2967(5)
	B	0.44(2)	1.06(2)	1.32(2)	1.88(2)	0.61(2)	1.07(3)	1.42(3)	1.70(4)	0.53(3)	1.32(3)	1.71(3)	2.03(4)
O(3)	x	0.3565(2)	0.3565(1)	0.3565(2)	0.3562(2)	0.3537(2)	0.3530(2)	0.3527(2)	0.3520(3)	0.3518(2)	0.3514(2)	0.3511(2)	0.3507(2)
	y	0.9871(2)	0.9886(2)	0.9896(2)	0.9911(2)	0.0072(2)	0.0069(2)	0.0065(2)	0.0062(3)	0.0079(2)	0.0076(2)	0.0074(2)	0.0070(3)
	z	0.0578(3)	0.0546(2)	0.0526(3)	0.0495(3)	0.0060(3)	0.0057(3)	0.0057(4)	0.0048(4)	0.0118(4)	0.0112(4)	0.0098(4)	0.0093(4)
	B	0.41(2)	1.05(2)	1.33(2)	1.86(3)	0.55(2)	1.00(3)	1.27(3)	1.52(4)	0.52(3)	1.15(3)	1.50(3)	1.82(3)
Si	x	0.2941(1)	0.2943(0)	0.2943(1)	0.2943(1)	0.2906(1)	0.2904(1)	0.2903(1)	0.2902(1)	0.2905(1)	0.2904(1)	0.2902(1)	0.2902(1)
	y	0.0935(1)	0.0932(0)	0.0931(1)	0.0928(1)	0.0933(1)	0.0931(1)	0.0928(1)	0.0926(1)	0.0894(1)	0.0891(1)	0.0889(1)	0.0888(1)
	z	0.2560(1)	0.2547(1)	0.2537(1)	0.2522(1)	0.2277(1)	0.2270(1)	0.2264(1)	0.2258(2)	0.2351(1)	0.2338(1)	0.2332(1)	0.2327(1)
	B	0.15(1)	0.53(1)	0.63(1)	0.95(1)	0.34(1)	0.62(1)	0.79(2)	0.95(2)	0.29(1)	0.69(1)	0.91(1)	1.12(1)
M(1)	x	0.0	0.0	0.0	0.0	0.0	0.0	0.0	0.0	0.0	0.0	0.0	0.0
	y	0.9066(1)	0.9059(1)	0.9054(1)	0.9044(1)	0.9058(1)	0.9050(1)	0.9043(1)	0.9039(2)	0.8989(1)	0.8979(1)	0.8974(1)	0.8969(1)
	z	0.2500	0.2500	0.2500	0.2500	0.2500	0.2500	0.2500	0.2500	0.2500	0.2500	0.2500	0.2500
	B	0.17(1)	0.57(1)	0.71(1)	1.07(1)	0.37(1)	0.70(2)	0.90(2)	1.12(2)	0.37(1)	0.78(1)	1.04(1)	1.30(1)
M(2)	x	0.0	0.0	0.0	0.0	0.0	0.0	0.0	0.0	0.0	0.0	0.0	0.0
	y	0.2752(9)	0.2758(7)	0.2750(9)	0.2769(10)	0.3005(2)	0.3006(2)	0.3007(2)	0.3008(3)	0.2999(2)	0.3000(2)	0.3001(3)	0.3002(3)
	z	0.2500	0.2500	0.2500	0.2500	0.2500	0.2500	0.2500	0.2500	0.2500	0.2500	0.2500	0.2500
	B	1.1(1)	2.19(8)	2.83(11)	4.13(14)	1.00(2)	1.93(3)	2.48(4)	3.06(5)	0.98(3)	2.24(3)	2.99(4)	3.58(5)

[a] Data from Clark et al (1969).

[b] Errors in parentheses are one standard deviation.

TABLE A-3, Continued

Atom	Parameter	Ureyite 24°C[a]	Ureyite 400°C	Ureyite 600°C	Diopside 24°C[a]	Diopside 400°C	Diopside 700°C	Diopside 850°C	Diopside 1000°C	Hedenbergite 24°C	Hedenbergite 400°C	Hedenbergite 600°C	Hedenbergite 800°C	Hedenbergite 900°C	Hedenbergite 1000°C
O(1)	x	0.1140(3)	0.1139(4)	0.1140(4)	0.1156(1)	0.1160(2)	0.1164(2)	0.1161(2)	0.1164(2)	0.1197(1)	0.1195(2)	0.1194(1)	0.1195(2)	0.1193(2)	0.1196(3)
	y	0.0791(3)	0.0794(4)	0.0782(4)	0.0873(1)	0.0868(2)	0.0864(2)	0.0863(2)	0.0864(2)	0.0904(2)	0.0898(2)	0.0894(2)	0.0892(2)	0.0889(3)	0.0890(3)
	z	0.1374(5)	0.1369(8)	0.1362(7)	0.1422(2)	0.1424(4)	0.1423(4)	0.1418(3)	0.1423(4)	0.1525(3)	0.1519(3)	0.1514(3)	0.1517(4)	0.1506(4)	0.1502(5)
	B	0.42(4)	1.04(6)	0.94(6)	0.33(2)	1.05(3)	1.52(3)	1.65(2)	1.95(3)	0.58(2)	1.08(2)	1.39(3)	1.69(3)	1.91(3)	2.02(4)
O(2)	x	0.3599(3)	0.3607(4)	0.3611(5)	0.3611(1)	0.3611(2)	0.3604(2)	0.3607(2)	0.3607(3)	0.3627(2)	0.3619(2)	0.3620(2)	0.3618(3)	0.3617(3)	0.3617(3)
	y	0.2583(3)	0.2571(5)	0.2573(5)	0.2500(1)	0.2486(2)	0.2477(2)	0.2468(2)	0.2464(3)	0.2461(2)	0.2449(2)	0.2444(2)	0.2436(2)	0.2429(3)	0.2428(3)
	z	0.3037(6)	0.3012(9)	0.3025(9)	0.3180(3)	0.3163(4)	0.3149(4)	0.3144(3)	0.3143(5)	0.3228(3)	0.3211(4)	0.3200(4)	0.3193(5)	0.3188(5)	0.3173(6)
	B	0.55(4)	1.32(7)	1.44(7)	0.46(2)	1.39(3)	1.96(4)	2.23(3)	2.62(4)	0.77(2)	1.46(3)	1.84(3)	2.30(4)	2.49(4)	2.76(6)
O(3)	x	0.3531(3)	0.3521(4)	0.3519(4)	0.3505(1)	0.3501(2)	0.3495(2)	0.3492(2)	0.3487(2)	0.3502(1)	0.3497(2)	0.3494(2)	0.3490(2)	0.3486(2)	0.3484(3)
	y	0.0105(3)	0.0099(5)	0.0094(5)	0.0176(1)	0.0165(2)	0.0157(2)	0.0151(2)	0.0146(3)	0.0198(2)	0.0180(2)	0.0172(2)	0.0164(3)	0.0162(2)	0.0160(3)
	z	0.0066(6)	0.0062(9)	0.0074(8)	0.9953(2)	0.9961(4)	0.9971(4)	0.9976(3)	-0.0024(4)	0.9932(3)	0.9949(3)	0.9969(3)	0.9976(4)	0.9973(4)	0.9976(5)
	B	0.53(3)	1.26(6)	1.29(6)	0.39(2)	1.22(3)	1.71(3)	1.86(3)	2.14(4)	0.65(2)	1.20(3)	1.52(3)	1.86(3)	2.03(4)	2.22(5)
Si	x	0.2921(1)	0.2920(1)	0.2921(2)	0.2862(1)	0.2862(1)	0.2861(1)	0.2861(1)	0.2859(1)	0.2878(1)	0.2875(1)	0.2875(1)	0.2872(1)	0.2872(1)	0.2871(1)
	y	0.0918(1)	0.0918(2)	0.0912(2)	0.0933(1)	0.0929(1)	0.0925(1)	0.0925(1)	0.0924(1)	0.0924(1)	0.0921(1)	0.0918(1)	0.0916(1)	0.915(1)	0.0915(1)
	z	0.2333(2)	0.2328(3)	0.2324(3)	0.2293(1)	0.2294(1)	0.2294(1)	0.2293(1)	0.2292(1)	0.2326(1)	0.2329(1)	0.2329(1)	0.2324(1)	0.2327(1)	0.2327(2)
	B	0.36(2)	0.77(3)	0.83(3)	0.228(7)	0.80(1)	1.12(2)	1.18(1)	1.37(1)	0.39(1)	0.75(1)	0.96(1)	1.17(1)	1.29(2)	1.41(2)
M(1)	x	0.0	0.0	0.0	0.0	0.0	0.0	0.0	0.0	0.0	0.0	0.0	0.0	0.0	0.0
	y	0.9076(1)	0.9072(1)	0.9066(1)	0.9082(1)	0.9072(1)	0.9069(2)	0.9066(1)	0.9063(2)	0.9075(0)	0.9064(1)	0.9057(1)	0.9054(1)	0.9051(1)	0.9049(1)
	z	0.2500	0.2500	0.2500	0.2500	0.2500	0.2500	0.2500	0.2500	0.2500	0.2500	0.2500	0.2500	0.2500	0.2500
	B	0.42(1)	0.81(3)	0.84(3)	0.26(1)	0.96(2)	1.40(2)	1.57(2)	1.89(2)	0.44(1)	0.93(1)	1.25(1)	1.54(1)	1.74(2)	1.96(2)
M(2)	x	0.0	0.0	0.0	0.0	0.0	0.0	0.0	0.0	0.0	0.0	0.0	0.0	0.0	0.0
	y	0.3008(3)	0.3001(4)	0.3010(4)	0.3015(1)	0.3008(1)	0.3005(1)	0.3003(1)	0.3001(1)	0.3003(1)	0.2993(1)	0.2990(1)	0.2989(1)	0.2987(1)	0.2984(1)
	z	0.2500	0.2500	0.2500	0.2500	0.2500	0.2500	0.2500	0.2500	0.2500	0.2500	0.2500	0.2500	0.2500	0.2500
	B	0.77(4)	1.91(7)	2.44(8)	0.514(7)	1.41(2)	2.14(2)	2.37(2)	2.83(2)	0.66(1)	1.40(1)	1.86(1)	2.31(2)	2.63(2)	2.87(3)

TABLE A-4. Si—O Interatomic Distances (Å) in Six Clinopyroxenes

Atoms	Spodumene 24°C[a]	Spodumene 300°C	Spodumene 460°C	Spodumene 760°C	Jadeite 24°C	Jadeite 400°C	Jadeite 600°C	Jadeite 800°C	Acmite 24°C[a]	Acmite 400°C	Acmite 600°C	Acmite 800°C
Si-O(1)	1.638(2)[b]	1.641(1)	1.640(1)	1.643(1)	1.637(2)	1.636(2)	1.637(2)	1.638(2)	1.629(2)	1.631(2)	1.633(2)	1.632(2)
-O(2)	1.586(2)	1.585(1)	1.584(2)	1.584(1)	1.594(2)	1.593(2)	1.594(2)	1.596(3)	1.598(2)	1.598(2)	1.598(2)	1.598(2)
-O(3C1)	1.622(2)	1.624(1)	1.624(2)	1.624(1)	1.629(2)	1.629(2)	1.629(2)	1.630(2)	1.637(2)	1.635(2)	1.641(2)	1.642(2)
-O(3C2)	1.626(2)	1.626(1)	1.627(2)	1.628(1)	1.639(2)	1.642(2)	1.643(2)	1.642(2)	1.646(2)	1.649(2)	1.647(2)	1.647(2)
mean	1.618	1.619	1.619	1.620	1.625	1.625	1.626	1.627	1.628	1.628	1.630	1.630

Atoms	Ureyite 24°C[a]	Ureyite 400°C	Ureyite 600°C	Diopside 24°C[a]	Diopside 400°C	Diopside 700°C	Diopside 850°C	Diopside 1000°C	Hedenbergite 24°C	Hedenbergite 400°C	Hedenbergite 600°C	Hedenbergite 800°C	Hedenbergite 900°C	Hedenbergite 1000°C
Si-O(1)	1.626(4)	1.635(4)	1.638(4)	1.602(2)	1.601(2)	1.600(2)	1.603(2)	1.602(2)	1.601(1)	1.602(2)	1.603(2)	1.603(2)	1.605(2)	1.603(3)
-O(2)	1.586(3)	1.586(4)	1.598(4)	1.585(1)	1.586(2)	1.586(2)	1.583(2)	1.586(2)	1.585(2)	1.582(2)	1.584(2)	1.583(2)	1.582(2)	1.582(3)
-O(3C1)	1.640(4)	1.639(4)	1.631(5)	1.664(2)	1.671(2)	1.670(2)	1.670(2)	1.671(2)	1.666(2)	1.671(2)	1.666(2)	1.665(2)	1.668(2)	1.669(3)
-O(3C2)	1.645(4)	1.646(5)	1.650(5)	1.687(2)	1.687(2)	1.688(2)	1.689(2)	1.690(2)	1.686(2)	1.684(2)	1.688(2)	1.689(2)	1.687(2)	1.687(3)
mean	1.624	1.627	1.629	1.635	1.636	1.636	1.636	1.637	1.635	1.635	1.635	1.635	1.636	1.635

[a]Data from Clark et al (1969).

[b]Errors in parentheses are one standard deviation.

TABLE A-5. O—O Interatomic Distances (Å) in Silicate Tetrahedra of Six Clinopyroxenes

	Spodumene				Jadeite				Acmite			
Atoms	24°C[a]	300°C	460°C	760°C	24°C	400°C	600°C	800°C	24°C[a]	400°C	600°C	800°C
O(1)-O(2)	2.742(2)[b]	2.747(2)	2.747(2)	2.752(2)	2.778(2)	2.780(2)	2.782(3)	2.786(3)	2.742(3)	2.750(2)	2.753(3)	2.756(3)
-O(3C1)	2.635(2)	2.640(2)	2.639(2)	2.640(2)	2.637(2)	2.634(2)	2.635(2)	2.634(2)	2.650(3)	2.647(2)	2.652(3)	2.647(3)
-O(3C2)	2.651(3)	2.651(2)	2.650(2)	2.651(2)	2.639(2)	2.638(2)	2.639(2)	2.635(3)	2.654(3)	2.657(2)	2.657(3)	2.655(3)
O(2)-O(3C1)	2.658(2)	2.655(2)	2.653(2)	2.650(2)	2.646(2)	2.644(2)	2.642(2)	2.645(3)	2.651(3)	2.649(3)	2.651(3)	2.653(3)
-O(3C2)	2.535(2)	2.535(2)	2.536(2)	2.537(2)	2.579(2)	2.581(2)	2.582(3)	2.582(3)	2.585(3)	2.583(3)	2.583(3)	2.582(3)
O(3C1)-O(3C2)	2.616(1)	2.619(1)	2.620(1)	2.622(1)	2.614(1)	2.619(1)	2.622(1)	2.627(1)	2.651(1)	2.652(1)	2.657(1)	2.659(1)
mean	2.640	2.641	2.641	2.642	2.649	2.649	2.650	2.652	2.656	2.656	2.659	2.659

	Ureyite			Diopside					Hedenbergite					
Atoms	24°C[a]	400°C	600°C	24°C[a]	400°C	700°C	850°C	1000°C	24°C	400°C	600°C	800°C	900°C	1000°C
O(1)-O(2)	2.736(5)	2.749(5)	2.764(6)	2.735(2)	2.736(3)	2.732(3)	2.737(2)	2.738(5)	2.722(2)	2.720(2)	2.724(3)	2.723(3)	2.726(3)	2.723(4)
-O(3C1)	2.644(5)	2.647(5)	2.641(6)	2.678(2)	2.683(3)	2.679(3)	2.680(2)	2.679(5)	2.687(2)	2.692(2)	2.688(2)	2.689(3)	2.687(3)	2.685(4)
-O(3C2)	2.636(7)	2.642(6)	2.646(5)	2.695(3)	2.689(3)	2.686(3)	2.689(2)	2.686(5)	2.696(2)	2.693(2)	2.695(2)	2.692(3)	2.692(3)	2.692(4)
O(2)-O(3C1)	2.657(4)	2.652(6)	2.660(6)	2.658(2)	2.664(2)	2.667(3)	2.666(2)	2.672(5)	2.658(2)	2.663(2)	2.661(3)	2.663(3)	2.663(3)	2.661(4)
-O(3C2)	2.583(4)	2.586(6)	2.590(6)	2.570(2)	2.575(2)	2.578(3)	2.574(2)	2.575(5)	2.574(2)	2.570(3)	2.574(3)	2.570(3)	2.570(3)	2.575(4)
O(3C1)-O(3C2)	2.643(5)	2.643(1)	2.645(1)	2.644(3)	2.650(1)	2.652(1)	2.654(1)	2.656(1)	2.647(1)	2.649(1)	2.651(1)	2.651(1)	2.653(1)	2.654(1)
mean	2.650	2.653	2.658	2.663	2.666	2.666	2.667	2.668	2.664	2.665	2.666	2.665	2.665	2.665

[a] Data from Clark et al (1969).
[b] Errors in parentheses are one standard deviation.

TABLE A-6. Interatomic Angles (°) in Tetrahedral Chains of Six Clinopyroxenes

	Spodumene				Jadeite				Acmite			
Angles	24°C[a]	300°C	460°C	760°C	24°C	400°C	600°C	800°C	24°C[a]	400°C	600°C	800°C
O(1)-Si-O(2)	116.5(1)[b]	116.7(1)	116.8(1)	117.0(1)	118.6(1)	118.9(1)	118.9(1)	119.0(1)	116.4(1)	116.8(1)	116.9(1)	117.1(1)
O(1)-Si-O(3C1)	107.9(1)	107.9(1)	107.9(1)	107.8(1)	107.7(1)	107.6(1)	107.6(1)	107.4(1)	108.5(1)	108.3(1)	108.2(1)	107.9(1)
O(1)-Si-O(3C2)	108.6(1)	108.5(6)	108.4(1)	108.3(1)	107.4(1)	107.2(1)	107.2(1)	106.9(1)	108.3(1)	108.2(1)	108.2(1)	108.1(1)
O(2)-Si-O(3C1)	111.9(1)	111.7(1)	111.6(1)	111.4(1)	110.4(8)	110.3(1)	110.2(1)	110.2(1)	110.1(1)	110.1(1)	109.9(1)	110.0(1)
O(2)-Si-O(3C2)	104.2(1)	104.3(1)	104.3(1)	104.4(1)	105.9(1)	105.8(1)	105.8(1)	105.8(1)	105.6(1)	105.4(1)	105.5(1)	105.4(1)
O(3C1)-Si-O(3C2)	107.3(1)	107.4(1)	107.4(1)	107.5(1)	106.3(1)	106.4(1)	106.5(1)	106.8(1)	107.7(1)	107.8(1)	107.8(1)	107.9(1)
mean	109.4	109.4	109.4	109.4	109.4	109.4	109.4	109.4	109.4	109.4	109.4	109.4
O3C2-O3C1-O3C2	170.5(2)	171.6(1)	172.3(2)	173.4(2)	174.6(1)	174.8(2)	175.1(2)	175.3(2)	174.0(2)	174.2(2)	174.4(2)	174.7(2)
Si-O3-Si	139.0(1)	139.3(1)	139.5(1)	139.7(1)	139.1(1)	139.4(1)	139.5(1)	139.8(2)	139.4(2)	139.5(1)	139.6(1)	139.8(1)

	Ureyite			Diopside					Hedenbergite					
Angles	24°C[a]	400°C	600°C	24°C[a]	400°C	700°C	850°C	1000°C	24°C	400°C	600°C	800°C	900°C	1000°C
O(1)-Si-O(2)	116.8(2)	117.2(2)	117.4(2)	118.3(1)	118.3(1)	118.1(1)	118.4(1)	118.3(1)	117.4(1)	117.3(1)	117.4(1)	117.4(1)	117.5(1)	117.6(2)
O(1)-Si-O(3C1)	108.1(2)	107.9(2)	107.8(2)	110.1(1)	110.1(1)	110.0(1)	109.9(1)	109.9(1)	110.6(1)	110.6(1)	110.6(1)	110.7(1)	110.3(1)	110.3(2)
O(1)-Si-O(3C2)	107.4(2)	107.3(2)	107.1(2)	110.0(1)	109.7(1)	109.5(1)	109.5(1)	109.4(1)	110.2(1)	110.0(1)	109.9(1)	109.7(1)	109.7(1)	109.7(2)
O(2)-Si-O(3C1)	110.9(2)	110.6(2)	110.9(2)	109.8(1)	109.8(1)	110.0(1)	110.0(1)	110.2(1)	109.7(1)	109.9(1)	109.9(1)	110.1(1)	110.1(1)	109.9(2)
O(2)-Si-O(3C2)	106.1(2)	106.3(2)	105.8(2)	103.5(1)	103.7(1)	103.9(1)	103.7(1)	103.6(1)	103.7(1)	103.7(1)	103.7(1)	103.5(1)	103.7(1)	103.9(2)
O(3C1)-Si-O(3C2)	107.1(2)	107.1(2)	107.4(2)	104.2(1)	104.2(1)	104.3(1)	104.4(1)	104.4(1)	104.3(1)	104.3(1)	104.4(1)	104.5(1)	104.5(1)	104.5(1)
mean	109.4	109.4	109.4	109.3	109.3	109.3	109.3	109.3	109.3	109.3	109.3	109.4	109.3	109.3
O3C2-O3C1-O3C2	172.1(2)	172.5(4)	172.8(4)	166.4(1)	167.1(2)	167.7(2)	168.2(2)	168.5(2)	164.5(1)	165.8(2)	166.4(2)	167.1(2)	167.2(2)	167.3(3)
Si-O3-Si	139.7(2)	140.2(3)	140.3(3)	135.93(9)	136.3(1)	136.8(1)	137.0(1)	137.3(1)	136.0(1)	136.4(1)	136.8(1)	137.1(1)	137.3(2)	137.4(2)

[a] Data from Clark et al (1969).
[b] Errors in parentheses are 1 standard deviation.

TABLE A-7. *M*(1)–O Interatomic Distances (Å) in Six Clinopyroxenes

	Spodumene M(1) = Al				Jadeite M(1) = Al				Acmite M(1) = Fe^{3+}			
Atoms	24°C[a]	300°C	460°C	760°C	24°C	400°C	600°C	800°C	24°C[a]	400°C	600°C	800°C
M(1)-O(1A1),(1B1)	1.997(2)[b]	2.005(1)	2.012(1)	2.023(1)	1.995(2)	2.008(2)	2.017(2)	2.022(2)	2.109(2)	2.120(2)	2.129(2)	2.136(2)
-O(1A2),(1B2)	1.943(2)	1.946(1)	1.948(1)	1.949(1)	1.940(1)	1.943(2)	1.946(2)	1.948(2)	2.029(2)	2.029(2)	2.032(2)	2.033(2)
-O(2C1),(2D1)	1.818(2)	1.823(1)	1.825(2)	1.830(2)	1.852(2)	1.857(2)	1.857(2)	1.858(3)	1.936(2)	1.937(2)	1.941(2)	1.943(2)
mean	1.919	1.925	1.928	1.934	1.929	1.936	1.940	1.943	2.025	2.029	2.034	2.037

	Ureyite M(1) = Cr			Diopside M(1) = Mg					Hedenbergite M(1) = Fe^{2+}					
Atoms	24°C[a]	400°C	600°C	24°C[a]	400°C	700°C	850°C	1000°C	24°C	400°C	600°C	800°C	900°C	1000°C
M(1)-O(1A1),(1B1)	2.039(3)	2.052(4)	2.054(4)	2.115(1)	2.135(2)	2.147(2)	2.150(2)	2.160(2)	2.163(1)	2.178(2)	2.187(2)	2.193(2)	2.198(2)	2.206(3)
-O(1A2),(1B2)	2.009(6)	2.012(4)	2.013(4)	2.065(3)	2.067(2)	2.070(2)	2.069(2)	2.075(2)	2.140(1)	2.137(2)	2.135(2)	2.138(2)	2.133(2)	2.133(3)
-O(2C1),(2D1)	1.947(3)	1.949(4)	1.947(4)	2.050(1)	2.063(2)	2.076(2)	2.081(2)	2.086(3)	2.087(1)	2.100(2)	2.102(2)	2.110(2)	2.116(2)	2.116(3)
mean	1.998	2.004	2.005	2.077	2.088	2.098	2.100	2.107	2.130	2.138	2.141	2.147	2.149	2.152

[a]Data from Clark et al (1969).
[b]Errors in parentheses are one standard deviation.

TABLE A-8. O—O Interatomic Distances (Å) in the *M*(1) Octahedra of Six Clinopyroxenes

	Spodumene				Jadeite				Acmite			
Atoms	24°C[a]	300°C	460°C	760°C	24°C	400°C	600°C	800°C	24°C[a]	400°C	600°C	800°C
O1A1-O1B1	2.694(4)[b]	2.705(2)	2.714(3)	2.727(3)	2.724(3)	2.742(3)	2.751(3)	2.760(4)	2.798(4)	2.809(3)	2.821(4)	2.835(4)
O2C1-O2D1	2.787(4)	2.786(2)	2.787(3)	2.791(3)	2.787(3)	2.788(4)	2.782(4)	2.782(5)	2.941(4)	2.932(4)	2.931(4)	2.929(5)
(2)O1A1-O2C1	2.661(2)	2.675(2)	2.683(2)	2.698(2)	2.710(2)	2.727(2)	2.741(3)	2.746(3)	2.860(3)	2.877(3)	2.891(3)	2.899(3)
(2)O1A1-O1A2	2.951(2)	2.953(1)	2.954(1)	2.955(1)	2.918(1)	2.921(1)	2.926(2)	2.928(2)	2.985(2)	2.984(2)	2.988(2)	2.988(2)
(2)O1A2-O2C1	2.705(2)	2.714(2)	2.719(2)	2.727(2)	2.682(2)	2.685(2)	2.684(3)	2.687(3)	2.819(3)	2.820(3)	2.822(3)	2.822(3)
(2)O1A2-O2D1	2.697(2)	2.708(2)	2.716(2)	2.729(2)	2.820(2)	2.838(2)	2.849(3)	2.858(3)	2.964(3)	2.979(3)	2.992(3)	3.004(3)
(2)O1A1-O1B2	2.504(3)	2.507(2)	2.510(3)	2.512(2)	2.462(3)	2.469(3)	2.476(3)	2.475(4)	2.639(4)	2.638(3)	2.642(4)	2.644(4)
mean	2.710	2.717	2.722	2.730	2.725	2.734	2.740	2.744	2.856	2.861	2.869	2.873

	Ureyite			Diopside					Hedenbergite					
Atoms	24°C[a]	400°C	600°C	24°C[a]	400°C	700°C	850°C	1000°C	24°C	400°C	600°C	800°C	900°C	1000°C
O1A1-O1B1	2.775(6)	2.785(8)	2.795(7)	2.781(3)	2.799(4)	2.814(4)	2.815(3)	2.821(4)	2.798(3)	2.808(3)	2.816(3)	2.819(4)	2.826(4)	2.837(5)
O2C1-O2D1	2.897(7)	2.880(8)	2.883(9)	2.981(3)	2.984(4)	2.998(4)	2.992(4)	2.996(5)	2.990(3)	3.008(4)	3.005(4)	3.011(5)	3.012(5)	3.009(7)
(2)O1A1-O2C1	2.815(5)	2.841(6)	2.835(6)	3.013(2)	3.049(3)	3.070(3)	3.085(2)	3.099(3)	3.113(2)	3.137(2)	3.150(3)	3.165(3)	3.178(3)	3.186(4)
(2)O1A1-O1A2	2.975(5)	2.981(4)	2.975(4)	3.051(3)	3.060(2)	3.064(2)	3.068(2)	3.074(2)	3.088(2)	3.093(2)	3.095(2)	3.098(2)	3.099(2)	3.103(3)
(2)O1A2-O2C1	2.797(5)	2.789(6)	2.798(6)	2.878(3)	2.892(3)	2.900(3)	2.905(2)	2.912(3)	2.940(2)	2.951(2)	2.953(3)	2.961(3)	2.963(3)	2.957(4)
(2)O1A2-O2D1	2.904(6)	2.921(6)	2.925(6)	2.979(3)	2.999(3)	3.021(3)	3.026(2)	3.036(3)	3.057(2)	3.074(2)	3.081(3)	3.093(3)	3.099(3)	3.105(4)
(2)O1A1-O1B2	2.617(7)	2.631(8)	2.624(7)	2.813(3)	2.821(4)	2.829(4)	2.826(3)	2.839(4)	2.976(3)	2.970(3)	2.968(4)	2.971(4)	2.965(4)	2.971(5)
mean	2.824	2.833	2.833	2.936	2.952	2.965	2.969	2.978	3.012	3.022	3.026	3.034	3.037	3.041

[a]Data from Clark et al (1969).
[b]Errors in parentheses are one standard deviation.

TABLE A-9. Interatomic Angles (°) in *M*(1) Octahedra in Six Clinopyroxenes

	Spodumene				Jadeite				Acmite			
Atoms	24°C[a]	300°C	460°C	760°C	24°C	400°C	600°C	800°C	24°C[a]	400°C	600°C	800°C
O1A2,O1B2	174.5(1)[b]	174.0(1)	173.5(1)	172.8(1)	170.8(1)	170.1(1)	169.8(1)	169.3(2)	168.7(1)	167.9(1)	167.5(1)	167.0(1)
(2)O1A1,O2D1	167.8(1)	168.0(1)	168.0(1)	168.0(1)	166.2(1)	166.1(1)	166.0(1)	165.9(1)	167.3(1)	167.3(1)	167.2(1)	167.2(1)
O1A1,O1B1	84.8(1)	84.9(1)	84.8(1)	84.8(1)	86.1(1)	86.1(1)	86.0(1)	86.1(1)	83.1(1)	83.0(1)	83.0(1)	83.1(1)
O2C1,O2D1	100.0(1)	99.7(1)	99.6(1)	99.4(1)	97.6(1)	97.3(1)	97.0(1)	96.9(2)	98.9(1)	98.4(1)	98.1(1)	97.9(1)
(2)O1A1,O2C1	88.3(1)	88.5(1)	88.6(1)	88.7(1)	89.5(1)	89.7(1)	89.9(1)	90.0(1)	89.9(1)	90.2(1)	90.4(1)	90.4(1)
(2)O1A1,O1A2	97.0(1)	96.7(1)	96.5(1)	96.1(1)	95.7(1)	95.4(1)	95.2(1)	95.0(1)	92.3(1)	91.9(1)	91.8(1)	91.5(1)
(2)O1A1,O1B2	78.9(1)	78.8(1)	78.7(1)	78.5(1)	77.5(1)	77.3(1)	77.3(1)	77.1(1)	79.2(1)	78.9(1)	78.8(1)	78.7(1)
(2)O1A2,O2C1	92.0(1)	92.1(1)	92.2(1)	92.3(1)	90.0(1)	89.9(1)	89.8(1)	89.8(1)	90.6(1)	90.6(1)	90.5(1)	90.5(1)
(2)O1A2,O2D1	91.6(1)	91.8(1)	92.0(1)	92.4(1)	96.1(1)	96.6(1)	97.0(1)	97.3(1)	96.7(1)	97.3(1)	97.7(1)	98.1(1)

	Ureyite			Diopside					Hedenbergite					
Atoms	24°C[a]	400°C	600°C	24°C[a]	400°C	700°C	850°C	1000°C	24°C	400°C	600°C	800°C	900°C	1000°C
O1A2,O1B2	173.4(2)	173.3(2)	172.4(2)	177.8(1)	177.1(1)	176.7(1)	176.5(1)	176.4(1)	179.0(1)	178.1(1)	177.6(1)	177.4(1)	177.1(1)	177.0(1)
(2)O1A1,O2D1	169.2(1)	169.1(2)	169.2(2)	171.3(1)	171.3(1)	171.3(1)	171.3(1)	171.3(1)	173.0(1)	172.7	172.6(1)	172.6(1)	172.6(1)	172.5(1)
O1A1,O1B1	85.8(2)	85.5(2)	85.8(2)	82.2(1)	81.9(1)	81.9(1)	81.8(1)	81.6(1)	80.6(1)	80.3(1)	80.2(1)	80.0(1)	80.0(1)	80.0(1)
O2C1,O2D1	96.1(2)	95.3(3)	95.5(3)	93.3(1)	92.6(1)	92.4(1)	91.9(1)	91.8(2)	91.5(1)	91.5(1)	91.3(1)	91.0(1)	90.8(2)	90.6(2)
(2)O1A1,O2C1	89.8(2)	90.5(2)	90.2(2)	92.6(1)	93.1(1)	93.3(1)	93.6(1)	93.8(1)	94.1(1)	94.3(1)	94.5(1)	94.7(1)	94.9(1)	94.9(1)
(2)O1A1,O1A2	94.6(1)	94.4(2)	94.0(2)	93.8(1)	93.5(1)	93.2(1)	93.1(1)	93.1(1)	91.7(1)	91.6(1)	91.5(1)	91.4(1)	91.4(1)	91.3(1)
(2)O1A1,O1B2	80.6(1)	80.7(2)	80.4(2)	84.6(1)	84.3(1)	84.3(1)	84.1(1)	84.2(1)	87.5(1)	87.0(1)	86.7(1)	86.6(1)	86.4(1)	86.4(1)
(2)O1A2,O2C1	89.8(2)	89.5(2)	89.9(2)	88.8(1)	88.9(1)	88.8(1)	88.8(1)	88.8(1)	88.1(1)	88.3(1)	88.4(1)	88.4(1)	88.4(1)	88.2(1)
(2)O1A2,O2D1	94.4(2)	95.0(2)	95.2(2)	92.8(1)	93.1(1)	93.6(1)	93.6(1)	93.7(1)	92.6(1)	93.0(1)	93.3(1)	93.5(1)	93.6(1)	93.9(1)

[a] Data from Clark et al (1969).

[b] Errors in parentheses are one standard deviation.

TABLE A-11. Magnitudes and Orientations of the Principal Axes of Thermal Ellipsoids in Six Clinopyroxenes

			Si				M(1)				M(2)			
Pyroxene	°C	Ellipsoid axis, r_i i	rms amplitude Å r_i	Angle (°) of r_i with a	b	c	rms amplitude Å r_i	Angle (°) of r_i with a	b	c	rms amplitude Å r_i	Angle (°) of r_i with a	b	c
Spodumene	24[a]	1	0.034(3)[b]	36(8)	55(6)	99(14)	0.041(4)	80(22)	90	30(22)	0.11(1)	17(27)	90	93(27)
		2	0.042(2)	77(14)	96(12)	171(14)	0.048(3)	10(22)	90	120(22)	0.12(1)	90	180	90
		3	0.051(2)	57(7)	144(6)	89(11)	0.051(3)	90	0	90	0.13(1)	107(27)	90	3
	300	1	0.074(1)	79(12)	79(6)	33(13)	0.081(2)	88(16)	90	22(16)	0.159(7)	77(20)	90	33(20)
		2	0.077(1)	27(6)	68(4)	122(13)	0.085(2)	178(16)	90	68(16)	0.166(8)	90	180	90
		3	0.093(1)	66(3)	155(3)	93(2)	0.088(2)	90	0	90	0.175(7)	167(21)	90	57(21)
	460	1	0.082(1)	143(12)	101(6)	37(14)	0.092(2)	142(34)	90	32(34)	0.182(9)	75(35)	90	35(35)
		2	0.085(1)	119(13)	110(4)	126(14)	0.094(2)	130(34)	90	120(34)	0.192(9)	90	180	90
		3	0.100(1)	69(3)	157(3)	87(3)	0.097(2)	90	0	90	0.194(9)	163(34)	90	53(34)
	760	1	0.100(1)	55(5)	67(2)	62(6)	0.112(1)	63(10)	90	46(10)	0.206(9)	70(9)	90	40(9)
		2	0.106(1)	46(5)	77(3)	151(6)	0.118(1)	26(10)	90	135(10)	0.222(10)	90	180	90
		3	0.122(1)	65(2)	153(2)	90(2)	0.119(1)	90	0	90	0.255(10)	160(9)	90	50(9)
Jadeite	24	1	0.049(2)	88(3)	86(4)	20(3)	0.055(3)	90(4)	90	18(4)	0.089(3)	75(2)	90	32(2)
		2	0.068(2)	75(7)	16(7)	99(5)	0.068(3)	90	180	90	0.097(3)	90	180	90
		3	0.078(2)	16(17)	106(7)	108(3)	0.080(2)	0(5)	90	108(4)	0.144(2)	165(2)	90	58(2)
	400	1	0.078(2)	79(4)	73(5)	33(5)	0.081(2)	80(4)	90	28(4)	0.125(3)	70(1)	90	38(1)
		2	0.089(2)	59(6)	39(6)	119(6)	0.096(2)	90	180	90	0.130(3)	90	180	90
		3	0.099(1)	34(5)	124(5)	104(4)	0.104(2)	170(4)	90	62(4)	0.202(2)	160(1)	90	52(1)
	600	1	0.089(2)	73(4)	71(4)	40(4)	0.095(2)	72(4)	90	36(4)	0.133(3)	70(1)	90	37(1)
		2	0.102(1)	49(9)	52(9)	128(5)	0.108(2)	90	180	90	0.150(3)	90	180	90
		3	0.108(1)	46(9)	136(8)	99(6)	0.116(2)	162(4)	90	54(4)	0.232(3)	160(1)	90	53(1)
	800	1	0.093(2)	87(3)	81(4)	23(4)	0.100(3)	82(3)	90	26(3)	0.148(4)	75(1)	90	33(1)
		2	0.112(2)	58(7)	34(7)	109(4)	0.120(3)	90	180	90	0.165(4)	90	180	90
		3	0.121(2)	33(7)	123(7)	102(3)	0.134(2)	172(3)	90	64(3)	0.259(4)	165(1)	90	57(1)

TABLE A-10. *M*(2)–O Interatomic Distances (Å) in Six Clinopyroxenes

Atoms	Spodumene M(2) = Li				Jadeite M(2) = Na				Acmite M(2) = Na			
	24°C[a]	300°C	460°C	760°C	24°C	400°C	600°C	800°C	24°C[a]	400°C	600°C	800°C
M(2)-O(1A1),(1B1)	2.105(6)[b]	2.119(5)	2.122(6)	2.146(7)	2.356(2)	2.370(2)	2.377(2)	2.387(3)	2.398(3)	2.413(2)	2.424(3)	2.435(3)
-O(2C2),(2D2)	2.278(2)	2.281(2)	2.281(2)	2.286(2)	2.412(2)	2.421(2)	2.430(2)	2.437(3)	2.415(2)	2.422(2)	2.431(2)	2.437(2)
-O(3C1),(3D1)	2.251(6)	2.268(5)	2.286(6)	2.296(7)	2.366(2)	2.374(2)	2.377(2)	2.382(3)	2.430(3)	2.438(2)	2.446(3)	2.451(3)
-O(3C2),(3D2)	3.144(5)	3.129(4)	3.124(5)	3.103(6)	2.740(2)	2.753(2)	2.761(2)	2.768(3)	2.831(3)	2.838(2)	2.842(2)	2.849(3)
mean of 6	2.211	2.223	2.230	2.243								
mean of 8					2.469	2.480	2.486	2.494	2.518	2.528	2.536	2.543

Atoms	Ureyite M(2) = Na			Diopside M(2) = Ca					Hedenbergite M(2) = Ca					
	24°C[a]	400°C	600°C	24°C[a]	400°C	700°C	850°C	1000°C	24°C	400°C	600°C	800°C	900°C	1000°C
M(2)-O(1A1),(1B1)	2.378(4)	2.381(5)	2.403(5)	2.360(1)	2.377(2)	2.391(2)	2.394(2)	2.399(2)	2.355(1)	2.364(2)	2.373(2)	2.379(2)	2.386(2)	2.388(3)
-O(2C2),(2D2)	2.389(7)	2.400(5)	2.399(4)	2.353(3)	2.357(2)	2.366(2)	2.368(2)	2.370(3)	2.341(1)	2.348(2)	2.352(2)	2.355(2)	2.357(3)	2.363(3)
-O(3C1),(3D1)	2.424(4)	2.440(5)	2.435(5)	2.561(2)	2.571(2)	2.578(2)	2.580(2)	2.586(3)	2.627(2)	2.628(2)	2.628(2)	2.629(2)	2.636(3)	2.639(3)
-O(3C2),(3D2)	2.764(4)	2.783(5)	2.790(5)	2.717(1)	2.749(2)	2.773(2)	2.784(2)	2.797(2)	2.720(1)	2.756(2)	2.778(2)	2.794(2)	2.803(2)	2.812(3)
mean of 6														
mean of 8	2.489	2.501	2.507	2.498	2.514	2.527	2.532	2.538	2.511	2.524	2.533	2.539	2.546	2.551

[a]Data from Clark et al (1969).
[b]Errors in parentheses are one standard deviation.

TABLE A-11, Continued

Pyroxene	°C	Ellipsoid axis, r_i i	O(1) rms amplitude Å r_i	O(1) Angle (°) of r_i with a	b	c	O(2) rms amplitude Å r_i	O(2) Angle (°) of r_i with a	b	c	O(3) rms amplitude Å r_i	O(3) Angle (°) of r_i with a	b	c
Spodumene	24[a]	1	0.042(6)[b]	61(14)	86(12)	49(15)	0.045(6)	132(6)	138(6)	76(5)	0.043(6)	96(12)	68(5)	26(5)
		2	0.057(5)	40(23)	64(29)	134(18)	0.079(8)	52(8)	125(8)	136(12)	0.061(5)	161(6)	76(6)	83(12)
		3	0.064(4)	115(25)	27(29)	73(22)	0.092(3)	66(9)	111(8)	50(12)	0.101(3)	108(4)	153(4)	66(3)
	300	1	0.079(3)	38(11)	87(5)	72(11)	0.083(3)	56(3)	35(2)	96(3)	0.084(3)	100(8)	66(2)	25(2)
		2	0.089(2)	55(11)	72(6)	155(10)	0.120(2)	51(4)	110(4)	150(5)	0.099(2)	165(6)	84(4)	84(7)
		3	0.106(2)	103(5)	18(6)	74(6)	0.138(2)	58(4)	117(3)	61(5)	0.152(2)	101(2)	155(2)	65(1)
	460	1	0.086(3)	18(7)	81(4)	95(8)	0.089(3)	52(2)	38(2)	99(3)	0.090(3)	112(5)	65(1)	25(2)
		2	0.101(3)	77(8)	77(8)	166(8)	0.134(3)	54(4)	114(3)	149(5)	0.114(3)	155(5)	89(3)	95(5)
		3	0.117(3)	102(4)	16(7)	76(8)	0.156(2)	58(4)	118(3)	61(5)	0.172(2)	102(2)	155(1)	65(1)
	760	1	0.100(3)	28(4)	85(3)	82(4)	0.109(3)	56(2)	35(2)	94(2)	0.110(3)	104(5)	65(1)	25(1)
		2	0.123(2)	65(5)	71(4)	160(4)	0.164(2)	49(4)	110(3)	148(6)	0.129(2)	161(4)	85(3)	88(5)
		3	0.145(2)	103(3)	20(4)	71(4)	0.180(2)	59(5)	117(3)	59(6)	0.204(2)	102(1)	154(1)	65(1)
Jadeite	24	1	0.063(4)	68(11)	93(9)	40(11)	0.073(4)	73(5)	32(13)	70(15)	0.058(5)	92(5)	78(5)	20(5)
		2	0.078(4)	22(12)	91(32)	130(11)	0.084(4)	83(8)	64(15)	153(13)	0.091(3)	150(34)	61(33)	82(11)
		3	0.083(4)	88(30)	3(11)	88(22)	0.104(3)	162(5)	72(6)	72(7)	0.096(3)	120(34)	149(31)	72(7)
	400	1	0.088(4)	52(12)	87(9)	56(13)	0.086(4)	66(3)	31(4)	80(5)	0.081(4)	96(5)	65(3)	28(3)
		2	0.099(3)	48(13)	60(10)	136(13)	0.117(3)	95(6)	68(5)	149(6)	0.113(3)	168(6)	83(5)	82(5)
		3	0.113(3)	115(9)	31(10)	67(9)	0.140(3)	156(3)	69(4)	61(6)	0.137(3)	100(6)	154(3)	64(3)
	600	1	0.094(4)	33(6)	88(5)	75(6)	0.101(4)	64(3)	28(3)	88(4)	0.094(4)	97(5)	64(3)	27(3)
		2	0.116(3)	64(8)	57(14)	145(13)	0.138(3)	91(7)	79(5)	159(7)	0.124(3)	166(5)	81(4)	84(5)
		3	0.126(3)	108(8)	33(14)	59(14)	0.157(3)	154(3)	64(3)	69(8)	0.156(3)	103(4)	153(3)	63(2)
	800	1	0.107(4)	68(9)	96(6)	40(9)	0.112(5)	68(3)	25(4)	86(5)	0.100(5)	104(4)	68(3)	23(3)
		2	0.125(4)	30(10)	67(10)	124(10)	0.146(4)	91(6)	78(5)	158(6)	0.141(4)	156(6)	77(6)	93(5)
		3	0.141(4)	109(10)	24(10)	71(7)	0.175(4)	158(3)	69(3)	68(6)	0.167(4)	109(7)	154(4)	68(3)

[a]Data from Clark et al (1969).
[b]Errors in parentheses are one standard deviation.

TABLE A-11, Continued

Pyroxene	v_C	Ellipsoid axis, r_i i	Si rms amplitude Å r_i	Si Angle (°) of r_i with a	Si b	Si c	M(1) rms amplitude Å r_i	M(1) Angle (°) of r_i with a	M(1) b	M(1) c	M(2) rms amplitude Å r_i	M(2) Angle (°) of r_i with a	M(2) b	M(2) c
Acmite	24[a]	1	0.040(3)	36(3)	77(10)	73(3)	0.054(2)	38(2)	90	69(2)	0.086(5)	90	0	90
		2	0.054(3)	99(8)	13(10)	97(5)	0.058(2)	90	180	90	0.086(5)	118(3)	90	134(3)
		3	0.081(2)	125(3)	87(4)	18(3)	0.088	128(2)	90	21(2)	0.149(3)	152(3)	90	44(3)
	400	1	0.082(2)	23(6)	75(2)	89(7)	0.091(1)	35(5)	90	73(5)	0.133(3)	69(2)	90	38(2)
		2	0.091(1)	72(7)	89(4)	178(5)	0.101(1)	55(5)	90	163(5)	0.151(3)	90	180	90
		3	0.107(1)	76(3)	165(2)	91(4)	0.106(1)	90	0	90	0.212(3)	159(2)	90	52(2)
	600	1	0.098(1)	55(21)	75(3)	55(22)	0.107(1)	55(7)	90	52(7)	0.148(3)	70(1)	90	38(1)
		2	0.101(1)	37(21)	85(6)	144(22)	0.114(1)	35(7)	90	142(7)	0.174(3)	90	180	90
		3	0.122(1)	77(3)	164(2)	85(3)	0.122(1)	90	0	90	0.248(3)	160(1)	90	52(1)
	800	1	0.106(1)	29(5)	73(2)	84(6)	0.118(1)	43(3)	90	65(3)	0.169(3)	70(1)	90	37(1)
		2	0.116(1)	67(6)	91(3)	174(5)	0.131(1)	47(3)	90	155(3)	0.185(3)	90	180	90
		3	0.134(1)	74(2)	163(2)	88(3)	0.135(1)	90	0	90	0.271(3)	160(1)	90	53(1)
Ureyite	24[a]	1	0.043(5)	89(4)	83(6)	20(4)	0.054(3)	91(3)	90	16(3)	0.057(8)	75(3)	90	33(3)
		2	0.071(3)	78(13)	14(12)	100(7)	0.075(2)	90	180	90	0.080(6)	90	180	90
		3	0.081(3)	12(13)	102(13)	107(5)	0.086(2)	1(3)	90	106(3)	0.140(5)	165(3)	90	57(3)
	400	1	0.078(4)	40(17)	50(17)	103(5)	0.087(3)	90	0	90	0.114(7)	90	0	90
		2	0.087(4)	50(17)	140(17)	103(5)	0.087(3)	180(3)	90	72(3)	0.139(6)	116(4)	90	137(4)
		3	0.125(3)	89(3)	92(3)	18(3)	0.126(2)	90(3)	90	18(3)	0.201(6)	154(4)	90	47(4)
	600	1	0.087(4)	158(11)	111(12)	67(6)	0.091(3)	90	0	90	0.129(7)	90	0	90
		2	0.101(4)	71(12)	157(12)	108(9)	0.098(3)	180(6)	90	73(5)	0.152(6)	114(3)	90	139(3)
		3	0.117(3)	79(5)	99(8)	30(7)	0.119(3)	90(5)	90	17(5)	0.230(6)	156(3)	90	49(3)
Diopside	24[a]	1	0.049(2)	27(17)	72(20)	85(9)	0.052(3)	56(10)	90	49(10)	0.066(1)	66(1)	90	39(1)
		2	0.053(2)	67(20)	155(17)	106(11)	0.055(3)	90	180	90	0.068(1)	90	180	90
		3	0.059(1)	105(8)	107(11)	17(11)	0.065(2)	146(10)	90	41(10)	0.103(1)	156(1)	90	50(1)
	400	1	0.089(2)	46(7)	54(8)	77(3)	0.103(3)	63(6)	90	43(6)	0.109(2)	90	0	90
		2	0.097(2)	123(7)	36(8)	94(4)	0.105(3)	90	180	90	0.115(2)	115(1)	90	139(1)
		3	0.113(1)	118(3)	94(4)	13(3)	0.121(2)	153(6)	90	47(6)	0.169(1)	155(1)	90	49(1)

TABLE A-11, Continued

Pyroxene	v_C	Ellipsoid axis, r_i i	Si rms amplitude Å r_i	Si Angle (°) of r_i with a	Si b	Si c	M(1) rms amplitude Å r_i	M(1) Angle (°) of r_i with a	M(1) b	M(1) c	M(2) rms amplitude Å r_i	M(2) Angle (°) of r_i with a	M(2) b	M(2) c
Diopside	700	1	0.104(1)	22(3)	69(3)	98(2)	0.128(2)	42(13)	90	64(13)	0.139(1)	90	0	90
		2	0.121(1)	68(3)	155(4)	108(6)	0.135(2)	49(13)	90	155(13)	0.143(1)	114(1)	90	140(1)
		3	0.131(1)	92(3)	104(5)	19(5)	0.137(2)	90	0	90	0.203(1)	156(1)	90	50(1)
	850	1	0.117(1)	22(21)	69(10)	99(37)	0.128(2)	81(4)	90	25(4)	0.143(1)	72(1)	90	34(1)
		2	0.118(1)	76(29)	103(12)	166(15)	0.147(2)	90	180	90	0.147(1)	90	180	90
		3	0.131(1)	72(3)	154(3)	78(3)	0.147(2)	173(10)	90	67(10)	0.218(1)	162(1)	90	56(1)
	1000	1	0.122(1)	22(5)	74(3)	91(5)	0.141(2)	77(5)	90	29(5)	0.154(1)	71(1)	90	35(1)
		2	0.132(1)	71(5)	108(6)	162(6)	0.160(2)	90	180	90	0.162(1)	90	180	90
		3	0.141(1)	80(3)	156(5)	72(6)	0.161(2)	168(5)	90	62(5)	0.240(1)	161(1)	90	55(1)
Hedenbergite	24	1	0.065(2)	102(11)	50(8)	40(8)	0.070(1)	90	0	90	0.079(1)	69(2)	90	35(2)
		2	0.071(2)	168(15)	101(21)	80(21)	0.075(1)	120(12)	90	135(12)	0.084(1)	90	180	90
		3	0.073(2)	84(33)	137(13)	52(11)	0.078(1)	150(12)	90	45(12)	0.108(1)	159(2)	90	55(2)
	400	1	0.093(1)	86(24)	68(13)	29(25)	0.103(1)	63(3)	90	42(3)	0.110(1)	68(1)	90	37(1)
		2	0.095(1)	152(9)	114(13)	63(27)	0.108(1)	90	180	90	0.119(1)	90	180	90
		3	0.102(1)	62(8)	146(7)	80(7)	0.115(1)	153(3)	90	48(3)	0.164(1)	158(1)	90	53(1)
	600	1	0.104(1)	98(10)	80(6)	12(9)	0.117(1)	75(2)	90	30(2)	0.126(1)	71(1)	90	34(1)
		2	0.109(1)	157(7)	112(6)	80(10)	0.127(1)	90	180	90	0.136(1)	90	180	90
		3	0.117(1)	69(6)	155(6)	83(4)	0.133(1)	165(2)	90	60(2)	0.190(1)	161(8)	90	56(1)
	800	1	0.113(1)	49(7)	64(3)	65(8)	0.129(1)	71(2)	90	34(2)	0.140(1)	70(1)	90	35(1)
		2	0.121(1)	51(7)	83(6)	155(8)	0.140(1)	90	180	90	0.150(1)	90	180	90
		3	0.130(1)	66(4)	153(3)	85(5)	0.149(1)	161(2)	90	56(2)	0.213(1)	160(1)	90	55(1)
	900	1	0.121(1)	83(10)	78(5)	26(11)	0.134(1)	72(2)	90	33(2)	0.150(1)	70(1)	90	35(1)
		2	0.126(1)	23(6)	70(6)	115(11)	0.152(1)	90	180	90	0.158(1)	90	180	90
		3	0.137(1)	68(5)	156(5)	87(4)	0.158(1)	162(2)	90	57(2)	0.228(1)	160(1)	90	55(1)
	1000	1	0.124(2)	99(9)	74(4)	18(5)	0.145(1)	73(2)	90	32(2)	0.153(2)	70(1)	90	35(1)
		2	0.132(2)	169(7)	99(6)	81(8)	0.160(1)	90	180	90	0.168(2)	90	180	90
		3	0.144(2)	84(6)	161(4)	75(4)	0.167(1)	163(2)	90	58(2)	0.240(2)	160(1)	90	55(1)

TABLE A-11, Continued

Pyroxene	t_C	Ellipsoid axis, r_i i	O(1) rms amplitude Å r_i	O(1) Angle (°) of r_i with a	b	c	O(2) rms amplitude Å r_i	O(2) Angle (°) of r_i with a	b	c	O(3) rms amplitude Å r_i	O(3) Angle (°) of r_i with a	b	c
Acmite	24[a]	1	0.041(8)	37(5)	82(11)	71(5)	0.045(8)	61(6)	30(7)	89(4)	0.064(6)	41(16)	87(19)	67(15)
		2	0.069(5)	90(10)	12(10)	102(9)	0.081(5)	132(7)	61(7)	109(8)	0.074(5)	63(20)	140(8)	125(13)
		3	0.092(4)	127(5)	80(9)	22(6)	0.107(4)	124(7)	81(5)	19(8)	0.101(4)	118(6)	130(7)	44(7)
	400	1	0.084(4)	24(7)	82(4)	85(9)	0.097(4)	49(3)	41(3)	95(3)	0.101(4)	6(243)	92(140)	102(306)
		2	0.103(3)	72(9)	70(5)	160(5)	0.141(3)	59(36)	109(33)	156(53)	0.102(4)	83(251)	115(5)	154(92)
		3	0.132(3)	105(4)	22(5)	70(5)	0.144(3)	56(34)	125(22)	66(54)	0.152(3)	94(3)	155(3)	66(3)
	600	1	0.102(4)	25(10)	88(4)	83(10)	0.110(4)	55(3)	36(3)	94(3)	0.110(4)	88(13)	71(3)	27(9)
		2	0.117(3)	66(10)	77(5)	165(7)	0.159(3)	73(14)	95(10)	175(9)	0.122(3)	170(3)	81(3)	74(6)
		3	0.148(3)	98(4)	13(5)	77(5)	0.167(3)	40(8)	125(3)	88(18)	0.173(3)	99(3)	159(2)	69(2)
	800	1	0.108(4)	23(5)	83(3)	85(5)	0.117(4)	54(2)	37(2)	92(3)	0.126(4)	95(18)	68(3)	25(8)
		2	0.135(3)	71(6)	71(5)	161(5)	0.177(3)	59(40)	103(31)	160(54)	0.135(3)	173(13)	87(7)	80(16)
		3	0.163(3)	103(3)	20(5)	71(5)	0.179(3)	51(37)	124(15)	70(55)	0.187(3)	95(3)	158(2)	68(2)
Ureyite	24[a]	1	0.047(10)	92(10)	101(11)	19(8)	0.062(9)	72(10)	48(22)	57(24)	0.047(10)	92(8)	70(7)	26(7)
		2	0.079(7)	133(32)	135(31)	87(15)	0.076(7)	75(13)	51(22)	141(23)	0.088(6)	164(22)	76(20)	80(13)
		3	0.088(6)	137(32)	47(31)	71(9)	0.106(6)	156(8)	66(8)	73(9)	0.102(6)	106(22)	155(13)	67(7)
	400	1	0.087(9)	161(14)	108(14)	70(6)	0.071(11)	65(6)	29(6)	84(4)	0.105(8)	143(16)	54(15)	67(8)
		2	0.112(7)	72(14)	162(14)	97(12)	0.130(7)	25(6)	115(6)	107(8)	0.126(7)	127(16)	139(17)	93(16)
		3	0.140(7)	86(7)	90(11)	22(7)	0.168(7)	94(7)	103(5)	19(8)	0.144(7)	91(12)	107(14)	23(9)
	600	1	0.072(11)	162(9)	102(8)	60(7)	0.080(11)	62(6)	28(6)	94(5)	0.108(9)	116(81)	47(31)	47(10)
		2	0.118(7)	108(9)	56(29)	130(23)	0.144(8)	31(8)	116(7)	121(15)	0.113(8)	154(80)	106(58)	94(57)
		3	0.128(7)	92(12)	37(28)	55(24)	0.165(7)	78(13)	101(8)	31(15)	0.157(7)	94(8)	132(6)	43(6)
Diopside	24[a]	1	0.051(4)	30(9)	98(9)	77(8)	0.050(4)	62(3)	30(4)	87(5)	0.058(4)	113(27)	59(6)	33(8)
		2	0.069(3)	65(14)	45(35)	132(34)	0.079(3)	103(7)	72(6)	146(8)	0.064(3)	156(26)	96(15)	98(23)
		3	0.073(3)	105(17)	46(35)	44(34)	0.094(3)	149(5)	67(4)	56(8)	0.085(3)	97(6)	148(5)	59(5)
	400	1	0.096(4)	23(6)	92(7)	83(6)	0.099(4)	68(3)	28(4)	81(4)	0.110(4)	147(45)	63(29)	58(25)
		2	0.119(4)	80(9)	21(16)	110(16)	0.137(4)	89(8)	73(5)	157(8)	0.113(4)	123(45)	124(25)	118(28)
		3	0.129(3)	111(6)	69(16)	22(15)	0.155(3)	158(3)	69(4)	69(8)	0.146(3)	96(4)	134(5)	45(5)

TABLE A-11, Continued

Pyroxene	t_C	Ellipsoid axis, r_i i	O(1) rms amplitude Å r_i	O(1) Angle (°) of r_i with a	b	c	O(2) rms amplitude Å r_i	O(2) Angle (°) of r_i with a	b	c	O(3) rms amplitude Å r_i	O(3) Angle (°) of r_i with a	b	c
Diopside	700	1	0.112(3)	7(4)	88(4)	99(4)	0.119(4)	63(2)	29(2)	87(3)	0.121(3)	138(9)	67(5)	43(5)
		2	0.149(3)	84(4)	76(40)	163(33)	0.165(3)	88(7)	79(5)	162(8)	0.139(3)	132(9)	115(5)	113(7)
		3	0.152(3)	93(6)	14(41)	76(41)	0.182(3)	153(2)	63(3)	73(8)	0.176(3)	90(3)	145(3)	56(3)
	850	1	0.121(3)	15(4)	90(3)	91(4)	0.127(3)	64(2)	29(2)	85(3)	0.120(3)	110(5)	64(2)	27(2)
		2	0.146(2)	75(5)	79(6)	169(6)	0.166(3)	85(3)	79(3)	164(3)	0.145(3)	159(4)	94(3)	95(4)
		3	0.164(2)	93(3)	11(6)	79(6)	0.203(2)	154(2)	64(2)	75(4)	0.188(2)	96(2)	153(2)	63(2)
	1000	1	0.132(3)	19(5)	89(3)	87(5)	0.139(3)	65(2)	33(2)	78(3)	0.129(3)	119(5)	63(2)	32(3)
		2	0.160(3)	71(5)	84(8)	173(8)	0.186(3)	83(5)	72(4)	160(5)	0.156(3)	150(5)	97(4)	103(5)
		3	0.176(3)	93(4)	6(8)	84(8)	0.213(3)	154(2)	64(3)	74(5)	0.200(3)	98(3)	152(2)	62(2)
Hedenbergite	24	1	0.073(4)	25(10)	100(7)	82(12)	0.080(4)	64(4)	32(5)	79(8)	0.076(4)	112(16)	62(6)	30(5)
		2	0.086(3)	70(12)	102(13)	167(13)	0.099(3)	80(8)	75(8)	165(8)	0.086(4)	158(16)	105(10)	92(14)
		3	0.097(3)	104(7)	164(11)	79(13)	0.115(3)	28(5)	118(5)	101(8)	0.108(3)	86(6)	148(5)	60(5)
	400	1	0.100(3)	21(6)	100(5)	86(7)	0.103(3)	67(3)	27(3)	83(4)	0.098(4)	108(8)	61(3)	30(3)
		2	0.121(3)	71(7)	91(18)	176(7)	0.141(3)	81(8)	80(5)	168(7)	0.116(3)	160(8)	92(5)	95(7)
		3	0.128(3)	81(7)	10(5)	90(16)	0.157(3)	25(4)	115(3)	100(8)	0.150(3)	97(4)	151(3)	61(3)
	600	1	0.114(3)	24(7)	93(4)	81(7)	0.116(3)	66(2)	29(3)	80(4)	0.108(3)	107(5)	64(2)	26(2)
		2	0.132(3)	66(7)	76(8)	163(8)	0.155(3)	81(5)	76(4)	165(4)	0.136(3)	163(5)	96(4)	91(5)
		3	0.149(3)	94(5)	14(7)	76(8)	0.181(3)	25(3)	115(2)	101(5)	0.167(3)	92(4)	153(2)	64(2)
	800	1	0.119(3)	20(5)	97(3)	86(5)	0.130(4)	64(2)	29(2)	85(3)	0.118(4)	102(6)	64(2)	26(2)
		2	0.146(3)	71(5)	85(6)	173(6)	0.177(3)	85(6)	78(4)	164(7)	0.144(3)	167(5)	90(4)	88(5)
		3	0.169(3)	86(3)	8(4)	84(6)	0.198(3)	153(3)	63(3)	75(8)	0.190(5)	96(3)	154(2)	64(2)
	900	1	0.131(3)	13(5)	85(3)	93(6)	0.141(4)	66(2)	27(3)	85(4)	0.118(4)	110(4)	59(2)	32(2)
		2	0.157(3)	78(6)	87(8)	176(7)	0.177(3)	91(5)	77(4)	159(5)	0.155(3)	159(4)	97(3)	95(4)
		3	0.175(3)	95(4)	5(5)	87(8)	0.209(3)	156(2)	67(2)	70(5)	0.198(3)	95(3)	148(2)	58(2)
	1000	1	0.133(4)	29(8)	89(3)	76(8)	0.146(5)	63(3)	33(3)	81(5)	0.130(5)	98(6)	62(2)	29(3)
		2	0.154(4)	61(8)	88(5)	166(8)	0.188(4)	86(6)	73(5)	160(6)	0.158(4)	172(6)	91(4)	83(6)
		3	0.188(4)	92(4)	2(5)	88(5)	0.219(4)	153(3)	63(3)	72(6)	0.206(4)	93(4)	152(2)	62(2)

References

ALEKHINA, L. G., AND M. V. AKHMANOVA (1971) The vibrational spectra of structural groups in orthosilicates. *Geochem. Int.* **8,** 504–510.

BADGER, R. M. (1935) The relationship between the internuclear distances and force constants of molecules and its application to polyatomic molecules. *J. Chem. Phys.* **3,** 710–714.

BROWN, G. E., AND G. V. GIBBS (1970) Stereochemistry and ordering in the tetrahedral portion of silicates. *Amer. Mineral.* **55,** 1587–1607.

———, C. T. PREWITT, J. J. PAPIKE, AND S. SUENO (1972) A comparison of the structures of low and high pigeonite. *J. Geophys. Res.* **77,** 5778–5789.

———, S. SUENO, AND C. T. PREWITT (1973) A new single-crystal heater for the precession camera and four-circle diffractometer. *Amer. Mineral.* **58,** 698–704.

BURNHAM, CHARLES W., JOAN R. CLARK, J. J. PAPIKE, AND C. T. PREWITT (1967) A proposed crystallographic nomenclature for clinopyroxene structures. *Z. Kristallogr.* **125,** 109–119.

BUSING, W. R., AND H. A. LEVY (1964) The effect of thermal motion on the estimation of bond lengths from diffraction measurements. *Acta Crystallogr.* **17,** 142–146.

CHRISTENSEN, A. N., AND R. G. HAZELL (1967) The crystal structure of $NaIn(SiO_3)_2$. *Acta Chem. Scand.* **21,** 1425–1429.

CLARK, JOAN R., D. E. APPLEMAN, AND J. J. PAPIKE (1969) Crystal-chemical characterization of clinopyroxenes based on eight new structure refinements. *Mineral. Soc. Amer. Spec. Pap.* **2,** 31–50.

DOYLE, P. A., AND P. A. TURNER (1968) Relativistic Hartree-Fock X-ray and electron scattering factors. *Acta Crystallogr.* **A24,** 390–397.

FREED, R. L., AND D. R. PEACOR (1967) Refinement of the crystal structure of johannsenite. *Amer. Mineral.* **52,** 709–720.

PAPIKE, J. J., MALCOLM ROSS, AND JOAN R. CLARK (1969) Crystal-chemical characterization of clinoamphiboles based on five new structure refinements. *Mineral. Soc. Amer. Spec. Pap.* **2,** 117–136.

———, C. T. PREWITT, S. SUENO, AND M. CAMERON (1973) Pyroxenes: Comparisons of real and ideal structural topologies. *Z. Kristallogr.* **69,** 254–273.

PREWITT, C. T., AND CHARLES W. BURNHAM (1966) The crystal structure of jadeite, $NaAlSi_2O_6$. *Amer. Mineral.* **51,** 956–975.

ROBINSON, K., G. V. GIBBS, AND P. H. RIBBE (1971) Quadratic elongation: a quantitative measure of distortion in coordination polyhedra. *Science,* **172,** 567–570.

SKINNER, B. J. (1966) *Handbook of Physical Constants.* Geol. Soc. Amer., pp. 76–96.

SMYTH, J. R. (1971) Protoenstatite: a crystal-structure refinement at 1100°C. *Z. Kristallogr.* **134,** 262–274.

———, AND CHARLES W. BURNHAM (1972) The crystal structures of high and low clinohypersthene. *Earth Planet. Sci. Lett.* **14,** 183–189.

SUENO, S., M. CAMERON, J. J. PAPIKE, AND C. T. PREWITT (1973) High-temperature crystal chemistry of tremolite. *Amer. Mineral.* **58,** 649–664.

TAKEDA, H. (1972) Crystallographic studies of coexisting aluminan orthopyroxenes and augite of high pressure origin. *J. Geophys. Res.* **77,** 5798–5811.

URUSOV, V. S. (1967) Chemical bonding in silica and silicates. *Geochem. Int.* **4,** 350–362.

VEBLEN, D. R., AND CHARLES W. BURNHAM (1969) The crystal structures of hedenbergite and ferrosilite (abstr.) *Can. Mineral.* **10,** 147.

WARREN, B., AND W. L. BRAGG (1928) The structure of diopside $CaMg(SiO_3)_2$. *Z. Kristallogr.* **69,** 168–193.

Manuscript received, November 6, 1972;
accepted for publication, January 30, 1973.